Global Biogeochemical Cycles®

RESEARCH ARTICLE
10.1029/2023GB007780

Special Section:
Regional Carbon Cycle Assessment and Processes - 2

Magnitude, Trends, and Variability of the Global Ocean Carbon Sink From 1985 to 2018

Tim DeVries[1,2], Kana Yamamoto[2,3], Rik Wanninkhof[4], Nicolas Gruber[5], Judith Hauck[6], Jens Daniel Müller[5], Laurent Bopp[7], Dustin Carroll[8,9], Brendan Carter[10,11], Thi-Tuyet-Trang Chau[12], Scott C. Doney[13], Marion Gehlen[12], Lucas Gloege[14,15], Luke Gregor[5], Stephanie Henson[16], Ji Hyun Kim[2,3], Yosuke Iida[17], Tatiana Ilyina[18,19], Peter Landschützer[18,20], Corinne Le Quéré[21], David Munro[22,23], Cara Nissen[6,24], Lavinia Patara[25], Fiz F. Pérez[26,27], Laure Resplandy[28], Keith B. Rodgers[29,30], Jörg Schwinger[31], Roland Séférian[32], Valentina Sicardi[33], Jens Terhaar[34,35,36], Joaquin Triñanes[4,37], Hiroyuki Tsujino[38], Andrew Watson[39], Sayaka Yasunaka[40,41], and Jiye Zeng[42]

[1]Department of Geography, University of California, Santa Barbara, Santa Barbara, CA, USA, [2]Earth Research Institute, University of California, Santa Barbara, Santa Barbara, CA, USA, [3]Interdepartmental Graduate Program in Marine Science, University of California, Santa Barbara, Santa Barbara, CA, USA, [4]Atlantic Oceanographic and Meteorological Laboratory, National Oceanic and Atmospheric Administration, Miami, FL, USA, [5]Environmental Physics, Institute of Biogeochemistry and Pollutant Dynamics, ETH Zurich, Zürich, Switzerland, [6]Alfred-Wegener-Institut, Helmholtz-Zentrum für Polar- und Meeresforschung, Bremerhaven, Germany, [7]LMD/IPSL, Ecole normale supérieure, Université PSL, CNRS, Sorbonne Université, Ecole Polytechnique, Paris, France, [8]Moss Landing Marine Laboratories, San José State University, Moss Landing, CA, USA, [9]Jet Propulsion Laboratory, California Institute of Technology, Pasadena, CA, USA, [10]Cooperative Institute for Climate, Ocean, and Ecosystem Studies, Seattle, WA, USA, [11]Pacific Marine Environmental Laboratory, National Oceanic and Atmospheric Administration, Seattle, WA, USA, [12]Laboratoire des Sciences du Climat et de l'Environnement, LSCE/IPSL, CEA-CNRS-UVSQ, Université Paris-Saclay, Gif-sur-Yvette, France, [13]Department of Environmental Sciences, University of Virginia, Charlottesville, VA, USA, [14]Lamont-Doherty Earth Observatory, Department of Earth and Environmental Sciences, Columbia University, New York, NY, USA, [15]Open Earth Foundation, Marina del Rey, CA, USA, [16]National Oceanography Centre, Southampton, UK, [17]Atmosphere and Ocean Department, Japan Meteorological Agency, Minato City, Japan, [18]Max Planck Institute for Meteorology, Hamburg, Germany, [19]Center for Earth System Research and Sustainability, Helmholtz-Zentrum Hereon, Universität Hamburg, Hamburg, Germany, [20]Flanders Marine Institute (VLIZ), Ostened, Belgium, [21]School of Environmental Sciences, University of East Anglia, Norwich, UK, [22]Cooperative Institute for Research in Environmental Sciences, University of Colorado, Boulder, CO, USA, [23]National Oceanic & Atmospheric Administration, Global Monitoring Laboratory (NOAA/GML), Boulder, CO, USA, [24]Department of Atmospheric and Oceanic Sciences and Institute of Arctic and Alpine Research, University of Colorado, Boulder, CO, USA, [25]GEOMAR Helmholtz-Zentrum für Ozeanforschung Kiel, Kiel, Germany, [26]Instituto de Investigaciones Marinas (IIM), CSIC, Vigo, Spain, [27]Oceans Department, Stanford University, Stanford, CA, USA, [28]Geosciences and High Meadows Environmental Institute, Princeton University, Princeton, NJ, USA, [29]Center for Climate Physics, Institute for Basic Science, Busan, South Korea, [30]Pusan National University, Busan, South Korea, [31]NORCE Climate & Environment, Bjerknes Centre for Climate Research, Bergen, Norway, [32]CNRM, Université de Toulouse, Météo-France, CNRS, Toulouse, France, [33]Barcelona Supercomputing Center, Climate Variability and Change Group, Barcelona, Spain, [34]Department of Marine Chemistry and Geochemistry, Woods Hole Oceanographic Institution, Woods Hole, MA, USA, [35]Climate and Environmental Physics, Physics Institute, University of Bern, Bern, Switzerland, [36]Oeschger Centre for Climate Change Research, University of Bern, Bern, Switzerland, [37]Department of Electronics and Computer Sciences, Universidad de Santiago de Compostela, Santiago de Compostela, Spain, [38]JMA Meteorological Research Institute, Tsukuba, Japan, [39]Global Systems Institute, University of Exeter, Norwich, UK, [40]Research Institute for Global Change, Japan Agency for Marine-Earth Science and Technology, Yokosuka, Japan, [41]Graduate School of Science, Tohoku University, Sendai, Japan, [42]Earth Systems Division, National Institute for Environmental Studies, Tsukuba, Japan

Key Points:

- The RECCAP2 global ocean analysis provides an authoritative multi-model and observation-based assessment of global ocean CO_2 uptake
- pCO_2-based products yield a mean sea-air CO_2 flux from 1985 to 2018 of -1.6 ± 0.2 PgC yr^{-1} with a trend of -0.61 PgC yr^{-1} $decade^{-1}$ since 2001
- Ocean anthropogenic CO_2 uptake averages -2.1–2.4 PgC yr^{-1} from 1985 to 2018, with a trend of -0.34–0.41 PgC yr^{-1} $decade^{-1}$ since 2001

Supporting Information:

Supporting Information may be found in the online version of this article.

Correspondence to:

T. DeVries,
tdevries@geog.ucsb.edu

Citation:

DeVries, T., Yamamoto, K., Wanninkhof, R., Gruber, N., Hauck, J., Müller, J. D., et al. (2023). Magnitude, trends, and variability of the global ocean carbon sink from 1985 to 2018. *Global Biogeochemical Cycles*, *37*, e2023GB007780. https://doi.org/10.1029/2023GB007780

Received 23 MAR 2023
Accepted 4 SEP 2023

Author Contributions:

Conceptualization: Tim DeVries, Rik Wanninkhof

Abstract This contribution to the RECCAP2 (REgional Carbon Cycle Assessment and Processes) assessment analyzes the processes that determine the global ocean carbon sink, and its trends and variability over the period 1985–2018, using a combination of models and observation-based products. The mean sea-air CO_2 flux from 1985 to 2018 is -1.6 ± 0.2 PgC yr^{-1} based on an ensemble of reconstructions of the history of sea surface pCO_2 (pCO_2 products). Models indicate that the dominant component of this flux is the net oceanic uptake of anthropogenic CO_2, which is estimated at -2.1 ± 0.3 PgC yr^{-1} by an ensemble of ocean biogeochemical models, and -2.4 ± 0.1 PgC yr^{-1} by two ocean circulation inverse models. The ocean also degasses about 0.65 ± 0.3 PgC yr^{-1} of terrestrially derived CO_2, but this process is not fully resolved by any of

Data curation: Kana Yamamoto, Jens Daniel Müller, Laurent Bopp, Dustin Carroll, Thi-Tuyet-Trang Chau, Scott C. Doney, Marion Gehlen, Lucas Gloege, Luke Gregor, Ji Hyun Kim, Yosuke Iida, Tatiana Ilyina, Peter Landschützer, Corinne Le Quéré, David Munro, Cara Nissen, Lavinia Patara, Laure Resplandy, Jörg Schwinger, Roland Séférian, Valentina Sicardi, Joaquin Triñanes, Hiroyuki Tsujino, Andrew Watson, Jiye Zeng
Formal analysis: Kana Yamamoto
Funding acquisition: Tim DeVries
Investigation: Tim DeVries, Kana Yamamoto, Laurent Bopp, Dustin Carroll, Thi-Tuyet-Trang Chau, Scott C. Doney, Lucas Gloege, Luke Gregor, Yosuke Iida, Tatiana Ilyina, Peter Landschützer, Corinne Le Quéré, David Munro, Cara Nissen, Lavinia Patara, Laure Resplandy, Jörg Schwinger, Roland Séférian, Valentina Sicardi, Joaquin Triñanes, Hiroyuki Tsujino, Andrew Watson, Jiye Zeng
Methodology: Tim DeVries, Nicolas Gruber, Judith Hauck, Jens Daniel Müller
Project Administration: Tim DeVries, Rik Wanninkhof, Nicolas Gruber, Judith Hauck, Jens Daniel Müller
Software: Kana Yamamoto
Supervision: Tim DeVries, Nicolas Gruber, Judith Hauck, Jens Daniel Müller
Visualization: Kana Yamamoto
Writing – original draft: Tim DeVries
Writing – review & editing: Tim DeVries, Kana Yamamoto, Rik Wanninkhof, Nicolas Gruber, Judith Hauck, Jens Daniel Müller, Laurent Bopp, Dustin Carroll, Brendan Carter, Thi-Tuyet-Trang Chau, Scott C. Doney, Marion Gehlen, Lucas Gloege, Luke Gregor, Stephanie Henson, Yosuke Iida, Tatiana Ilyina, Peter Landschützer, Corinne Le Quéré, David Munro, Cara Nissen, Lavinia Patara, Fiz F. Pérez, Laure Resplandy, Keith B. Rodgers, Jörg Schwinger, Roland Séférian, Valentina Sicardi, Jens Terhaar, Joaquin Triñanes, Hiroyuki Tsujino, Andrew Watson, Sayaka Yasunaka, Jiye Zeng

the models used here. From 2001 to 2018, the pCO_2 products reconstruct a trend in the ocean carbon sink of -0.61 ± 0.12 PgC yr^{-1} $decade^{-1}$, while biogeochemical models and inverse models diagnose an anthropogenic CO_2-driven trend of -0.34 ± 0.06 and -0.41 ± 0.03 PgC yr^{-1} $decade^{-1}$, respectively. This implies a climate-forced acceleration of the ocean carbon sink in recent decades, but there are still large uncertainties on the magnitude and cause of this trend. The interannual to decadal variability of the global carbon sink is mainly driven by climate variability, with the climate-driven variability exceeding the CO_2-forced variability by 2–3 times. These results suggest that anthropogenic CO_2 dominates the ocean CO_2 sink, while climate-driven variability is potentially large but highly uncertain and not consistently captured across different methods.

Plain Language Summary The second REgional Carbon Cycle Assessment and Processes effort, or RECCAP2, provides a comprehensive assessment of global and regional greenhouse gas budgets. This paper focuses on the ocean carbon sink, and investigates the processes that control its magnitude, trends and variability. Observation-based techniques estimate that the net transfer of CO_2 from the atmosphere to the ocean, averaged over 1985–2018, is 1.6 billion tonnes of carbon per year, and that oceanic CO_2 uptake is increasing by 0.61 billion tonnes of carbon per year each decade. Models say that most of this CO_2 entering the ocean, and its increase over time, is driven by anthropogenic CO_2 emissions, which causes the ocean to take up 2.1–2.4 billion tonnes of carbon per year. There are some hints that climate change might be accelerating ocean carbon uptake, but the errors in our estimates are too large to know for sure right now. Our methods and observations will have to be improved in order to better detect the impact of climate change on the ocean carbon sink.

1. Introduction

In the last decade (2012–2021) human activities have added 10.8 ± 0.8 Pg C yr^{-1} to the atmosphere as CO_2 (Friedlingstein et al., 2022), accounting for roughly half of the anthropogenic radiative forcing from well-mixed greenhouse gases (Forster et al., 2021). The ocean plays a critical role in mitigating climate change by absorbing much of these anthropogenic CO_2 emissions. The ocean's long-term capacity to take up anthropogenic CO_2 is limited only by its size and the CO_2 buffering capacity of seawater (Broecker et al., 1979; DeVries, 2022b; Revelle & Suess, 1957), and it is estimated that ultimately the ocean will absorb about 85% of anthropogenic CO_2 emissions (Archer, 2005; Broecker et al., 1979). In the short term, however, the rate of oceanic anthropogenic CO_2 uptake is limited by ocean circulation rates, in particular the ventilation rate of the ocean's intermediate and deeper layers (Iudicone et al., 2016; Sarmiento et al., 1992; Siegenthaler & Sarmiento, 1993), such that current rates of CO_2 uptake by the ocean average about 30% of anthropogenic carbon emissions (Crisp et al., 2022; Friedlingstein et al., 2022; Gruber et al., 2019a, 2019b, 2023; Sabine et al., 2004). Additionally, the net flow of CO_2 between the atmosphere and ocean is affected by perturbations to the natural carbon cycle due to climate variability and anthropogenic climate change (Gruber et al., 2019b; Le Quéré et al., 2007a; McKinley et al., 2017; Séférian et al., 2014), which can strengthen or weaken the global ocean carbon sink from year to year (Gruber et al., 2023; Le Quéré et al., 2010), and on longer timescales (Bernardello et al., 2014; Joos et al., 1999; McNeil & Matear, 2013).

Tracking the uptake of anthropogenic carbon by the ocean, and perturbations to the natural ocean carbon cycle, has been a focus of ocean biogeochemistry and climate science for many decades. Early efforts toward quantifying the oceanic sink for anthropogenic carbon relied on simple box or box-diffusion models with mixing rates calibrated using radioactive tracers (Bolin & Eriksson, 1959; Keeling, 1979; Oeschger et al., 1975). These simple box models progressed over time to three dimensional global ocean circulation-biogeochemical models (GOBMs) that could simulate the impacts of climate change on anthropogenic CO_2 uptake (Maier-Reimer & Hasselmann, 1987; Orr et al., 2001; Sarmiento et al., 1992). Another class of approaches relied primarily on geochemical observations to track changes in the ocean carbon sink. Some studies utilized atmospheric observations, such as O_2/N_2 ratios (e.g., Keeling et al., 1996), or changes in the atmospheric and oceanic stable carbon isotope ratio (e.g., Quay et al., 1992), to deduce the oceanic uptake of anthropogenic carbon. Other approaches applied ocean biogeochemical and transient tracers to remove the signals of natural variability from oceanic dissolved inorganic carbon (DIC) measurements in order to identify the anthropogenic perturbation (Brewer, 1978; Chen, 1982; Gruber et al., 1996; Lo Monaco et al., 2005; Sabine et al., 2004; Vázquez-Rodríguez et al., 2009). Still others used anthropogenic transient tracers such as chlorofluorocarbons (CFCs) to estimate ocean ventilation rates and anthropogenic CO_2 uptake by convolving ocean mixing rates with time-evolving atmospheric CO_2 concentrations

(Hall et al., 2002; Khatiwala et al., 2009; McNeil et al., 2003; Waugh et al., 2006). At the same time, a growing database of surface ocean seawater pCO_2 led to the development of methods that could estimate the contemporary ocean carbon sink at a global scale by scaling pCO_2 observations to a reference year and using a bulk formulation for air-sea CO_2 exchange (Takahashi et al., 1997, 2002, 2009).

This early work formed the basis for the ocean contribution to the first REgional Carbon Cycle Assessment and Processes (RECCAP), an international effort to quantify regional and global carbon fluxes and to better understand the processes governing the global sinks for anthropogenic CO_2 (Canadell et al., 2011). The RECCAP global ocean carbon sink assessment focused on the global ocean storage of anthropogenic carbon (Khatiwala et al., 2013) (hereafter, K2013) and on the magnitude, variability, and trends of air-sea CO_2 fluxes in the global ocean (Wanninkhof et al., 2013) (hereafter, W2013). The synthesis by K2013 focused on DIC inventory changes in the ocean, and provided an estimate of the total ocean anthropogenic carbon uptake since the start of the industrial revolution based on six observation-based approaches (including DIC-based approaches and tracer-constrained ocean mixing models), four versions of the Community Climate System Model GOBM, and a tracer-constrained global ocean data assimilation model (ECCO). W2013 focused on estimates of air-sea CO_2 fluxes derived from nine GOBMs, an empirical pCO_2-observation based approach (Park et al., 2010; Takahashi et al., 2009), an atmospheric and an ocean inversion, and two estimates based on atmospheric O_2/N_2 ratios.

Here, we provide an updated estimate of the global ocean carbon sink, its magnitude, trends, and variability over the period 1985–2018 as part of the RECCAP2 project. Our analysis takes advantage of improvements in methodologies for quantifying the ocean carbon sink since the first RECCAP assessment, and provides an analysis of the mechanisms driving changes in the ocean carbon sink over time. In addition to extending the analysis period to 2018, RECCAP2 uses a variety of models and observation-based products that were not available for RECCAP. As opposed to using variants of a single GOBM, we use an ensemble of 12 different GOBMs, which allows for more robust results and improved uncertainty quantification. The ECCO assimilation model, which was used in RECCAP, is also used here, but is improved by the assimilation of biogeochemical parameters. The empirical pCO_2-based approach of RECCAP that extended the Takahashi climatology is here replaced by an ensemble of 11 pCO_2-based interpolation products, many of which use machine learning approaches that were not available for RECCAP, allowing us to better capture temporal and spatial variability and to assess the robustness of the results. The tracer-constrained mixing models utilized in RECCAP are here replaced by an ocean circulation inverse model (OCIM) that estimates ocean mixing and ventilation by inverting distributions of six ocean circulation tracers. The DIC-observation based approach used in RECCAP, which provided estimates for the period from ~1800 to 1994 based on the C* approach (Gruber et al., 1996; Sabine et al., 2004), is here replaced by the extended multilinear regression method applied to the C* tracer to determine the anthropogenic carbon increase over the period 1994–2007 (Gruber et al., 2019a, 2019b). These improved models and data products allow better quantification of the global ocean carbon sink, and an in-depth analysis of the mechanisms contributing to its magnitude, variability and trends. It should be noted that the RECCAP2 project is distinct from but complements the Global Carbon Budget (GCB) project (Friedlingstein et al., 2022), which focuses only on the anthropogenically perturbed surface CO_2 fluxes from a global budgeting perspective. Also of note is that some of the approaches that were included as part of RECCAP are not considered for this RECCAP2 global assessment, such as estimates based on atmospheric CO_2 inversions (e.g., Jacobson et al., 2007) and atmospheric O_2/N_2 ratios (e.g., Manning & Keeling, 2006).

This paper is organized as follows. In Section 2, we provide background on the flux components of the ocean carbon sink, details of the methods used by each of the RECCAP2 approaches for estimating the ocean carbon sink, and information on the components that each approach captures. Section 3 discusses results of the RECCAP2 products' estimates of sea-air CO_2 fluxes (Section 3.1) and changes in ocean DIC concentrations (Section 3.2) over the period 1985–2018. In Section 4 we compare RECCAP2 results with those of the original RECCAP, consider remaining uncertainties and biases in the RECCAP2 products, and provide a "best estimate" of the contemporary global ocean CO_2 sink. Section 5 concludes with a summary of our main findings, and suggests several focus areas for future research.

2. Materials and Methods

2.1. Overview

Several different products were used to assess the global ocean carbon sink for RECCAP2. These products generally fall under one of two broad categories: models and observation-based products. We use two categories of

models, GOBMs and ocean data assimilation models. GOBMs are freely evolving dynamical ocean circulation models with a biogeochemical module, and use atmospheric reanalysis data as a boundary condition to force the ocean biogeochemical model. They have been used to assess the ocean carbon sink in the GCB (Friedlingstein et al., 2022; Hauck et al., 2020), and they form the ocean carbon cycle component of Earth System Models (e.g., Canadell et al., 2021; Schwinger et al., 2014; Terhaar et al., 2022). In contrast, ocean data assimilation models use observations of oceanic tracers to constrain the ocean circulation and/or biogeochemistry and have been used to provide data-constrained assessments of the ocean anthropogenic CO_2 uptake (DeVries, 2014) and the interannual variability of air-sea CO_2 fluxes (Carroll et al., 2022). Both categories of models provide estimates of air-sea CO_2 fluxes and the resulting changes in ocean interior DIC inventories over time.

We also use two categories of observation-based products, those based on surface ocean pCO_2, which determine the air-sea CO_2 flux, and those based on ocean-interior DIC, which estimate the oceanic accumulation of anthropogenic CO_2. pCO_2-observation products have been used in the GCB assessment (Friedlingstein et al., 2022) and include a variety of statistical, regression, and machine learning algorithms that are used to interpolate and extrapolate sparse observations of surface seawater pCO_2 to a regular grid with near-global coverage and monthly resolution, from which air-sea CO_2 fluxes are derived (Rodenbeck et al., 2015). The DIC-observation product used here is based on a multilinear regression model to estimate the change in anthropogenic DIC from 1994 to 2007 (Gruber et al., 2019a, 2019b) using observations gathered over the period from 1982 until 2013. A more detailed description of the products used is provided in Section 2.3 below.

2.2. Processes Contributing to Air-Sea CO_2 Fluxes and DIC Inventory Changes

When comparing results across the different products introduced above, it is important to keep in mind that different products resolve different aspects of the ocean carbon sink (i.e., the net uptake of CO_2 by the ocean), and capture different processes that affect the magnitude and variability of this sink. Here, we present a framework for analyzing changes in the ocean DIC inventory and air-sea CO_2 fluxes in terms of their driving processes, and Section 2.3 discusses the individual processes that are captured by each model or observation-based product.

At the local scale, changes in ocean DIC concentrations are related to fluxes across the air-sea and land-sea boundaries, and to the local physical and biological processes affecting DIC,

$$\frac{d\mathrm{DIC}}{dt} = \frac{1}{\Delta z}(f_{\mathrm{land-sea}} - f_{\mathrm{sea-air}}) + J_{\mathrm{DIC}} \tag{1}$$

where $f_{\mathrm{sea\text{-}air}}$ is the local net flux of CO_2 from the ocean to the atmosphere (mol m^{-2} yr^{-1}; positive into the atmosphere), $f_{\mathrm{land\text{-}sea}}$ is the local net flux of DIC (mol m^{-2} yr^{-1}) from the land to the ocean (positive into the ocean), and Δz is the depth interval over which $d\mathrm{DIC}/dt$ is expressed. The land-sea fluxes include all exchanges of carbon between oceanic DIC and solid terrestrial or sedimentary carbon reservoirs: for example, the input of DIC and the remineralization of organic carbon from rivers and submarine groundwaters (Cole et al., 2007), and the loss of DIC due to the burial of organic carbon and $CaCO_3$ in marine sediments (Burdige, 2007; Dunne et al., 2007). J_{DIC} represents the convergence of DIC due to biological transformation or physical transport (mol m^{-3} yr^{-1}), such as the formation and sinking of carbon bearing organic or inorganic particles, the transport of DIC by ocean currents, or the concentration and dilution of DIC by evaporation and precipitation.

In the global integral, internal ocean transports of DIC, J_{DIC}, are close to zero, so that the rate of change in the ocean DIC inventory (I_{DIC}; Pg C) is only related to the flux of CO_2 across the air-sea interface and at the land-sea boundary,

$$dI_{\mathrm{DIC}}/dt = F_{\mathrm{land-sea}} - F_{\mathrm{sea-air}} \tag{2}$$

where $F_{\mathrm{sea\text{-}air}}$ (Pg C yr^{-1}) is the global integral of $f_{\mathrm{sea-air}}$, and $F_{\mathrm{land\text{-}sea}}$ (Pg C yr^{-1}) is the global integral of $f_{\mathrm{land-sea}}$. At steady-state, as commonly assumed to be the case before human perturbations to the global carbon cycle, $dI_{\mathrm{DIC}}/dt = 0$ and the net flux of DIC from the land to the ocean and into/out of the sediments is balanced by the net flux of CO_2 from the ocean to the atmosphere, that is,

$$F_{\mathrm{sea-air,ss}} = F_{\mathrm{land-sea,ss}} \tag{3}$$

where the ss subscripts indicate a preindustrial steady-state.

In the contemporary ocean, the globally integrated sea-air CO_2 flux can be considered a combination of "anthropogenic" and "natural" components,

$$F_{\text{sea-air}} = F_{\text{ant}} + F_{\text{nat}} \tag{4}$$

Anthropogenic (ant) sea-air CO_2 fluxes include a component that is due only to rising atmospheric CO_2 in the absence of any climate variability, and a component that is due to the redistribution of anthropogenic DIC by climate variability and change, that is,

$$F_{\text{ant}} = F_{\text{ant,CO}_2} + F_{\text{ant,climate}} \tag{5}$$

Natural (nat) sea-air CO_2 fluxes include a preindustrial component that is balanced by land-sea fluxes at steady-state (see Equation 3), and a component due to the redistribution of natural (preindustrial) DIC driven by climate variability and change, that is,

$$F_{\text{nat}} = F_{\text{land-sea,ss}} + F_{\text{nat,climate}} \tag{6}$$

In this framework, any changes in air-sea CO_2 fluxes due to climate- or anthropogenic-driven land-sea DIC fluxes (e.g., Regnier et al., 2013, 2022) will be incorporated in the $F_{\text{nat, climate}}$ term. Thus, the net effect of climate variability and change on global air-sea CO_2 fluxes is the sum of its effect on natural and anthropogenic CO_2 fluxes,

$$F_{\text{climate}} = F_{\text{nat,climate}} + F_{\text{ant,climate}} \tag{7}$$

and the global sea-air CO_2 flux is given by

$$F_{\text{sea-air}} = F_{\text{ant,CO}_2} + F_{\text{land-sea,ss}} + F_{\text{climate}} \tag{8}$$

The same decomposition of sea-air CO_2 fluxes derived above for the globally integrated fluxes applies at the local scale. At a preindustrial steady-state ($d\text{DIC}/dt = 0$) Equation 1 yields

$$f_{\text{sea-air,ss}} = f_{\text{land-sea,ss}} + \Delta z \cdot J_{\text{DIC,ss}} \tag{9}$$

The contemporary net sea-air CO_2 flux is the sum of the steady-state fluxes (Equation 9) and the anthropogenic CO_2-driven fluxes and those fluxes driven by climate variability and change,

$$f_{\text{sea-air}} = f_{\text{ant,CO}_2} + f_{\text{climate}} + f_{\text{land-sea,ss}} + \Delta z \cdot J_{\text{DIC,ss}} \tag{10}$$

where f_{climate} is composed of natural and anthropogenic components as in Equation 7 for the global integral.

Analogously to the air-sea CO_2 fluxes, the transport of DIC can be decomposed into contributions from the preindustrial steady-state transports, and the transports driven by rising atmospheric CO_2 and by climate variability,

$$J_{\text{DIC}} = J_{\text{DIC,ss}} + J_{\text{DIC,ant,CO2}} + J_{\text{DIC,climate}} \tag{11}$$

Analogous to the air-sea fluxes (Equation 7), $J_{\text{DIC, climate}}$ has both anthropogenic and natural components.

For discussions in this manuscript, we adopt the following lexicon for the terms defined above: $f_{\text{sea-air}}$ is the "net sea-air CO_2 flux," $f_{\text{ant,CO2}}$ is the "anthropogenic CO_2-driven flux," f_{climate} is the "climate-driven CO_2 flux," $f_{\text{ant, climate}}$ is the "climate-driven anthropogenic CO_2 flux," $f_{\text{nat, climate}}$ is the "climate-driven natural CO_2 flux," and $f_{\text{land-sea}}$ is the "net land-sea carbon flux." Analogous terminology applies to the globally integrated fluxes, as well as the transports and DIC accumulation rates.

2.3. Description of Models and Observation-Based Products

2.3.1. Global Ocean Biogeochemical Models (GOBMs)

Here we use results from 12 GOBMs many of which have previously been used to assess the global ocean CO_2 uptake in the GCB (Friedlingstein et al., 2022). These models are forced with atmospheric CO_2 and reanalysis wind stress and buoyancy fluxes. In contrast to fully coupled Earth system models that capture only externally forced variability and trends (Taylor et al., 2012; Zelinka et al., 2020), the GOBMs can also provide hindcasts of the variability and trends of the ocean carbon sink that are due to internal climate variability.

10.1029/2023GB007780

Table 1
Components of the Sea-Air CO_2 Flux and Dissolved Inorganic Carbon Transport Represented by Each RECCAP2 Model or Observation-Based Product

Method		$f_{ant,CO2} + J_{DIC,ant,CO2}$	$f_{ant,\,climate} + J_{DIC,ant,climate}$	$f_{nat,\,climate} + J_{DIC,nat,climate}$	$f_{land\text{-}sea}$	$J_{DIC,ss}$	$f_{bias+drift} + J_{DIC,\,bias+drift}$
GOBMs and data assimilation models	Sim A	✓	✓[a]	✓[a]	[b]	✓	✓
	Sim B				[b]	✓	✓
	Sim C	✓			[b]	✓	✓
	Sim D			✓	[b]	✓	✓
pCO_2-observation products		✓	✓	✓	✓	✓	
DIC-observation product (eMLR-C*)		✓	✓				

[a]OCIM-v2014 does not represent these terms. OCIM-v2021 represents the effects of variable sea surface temperatures and wind speeds, but does not represent any variability in ocean circulation or biology like the GOBMs. See Section 2.3.2. [b]Some of the GOBMs partially represent land-sea carbon fluxes. See Table S1 in Supporting Information S1.

Many models first underwent a preindustrial spin-up using a constant atmospheric pCO_2 and climatological or repeated year forcing. Then, all models performed a historical simulation from the end of the preindustrial spin-up or from observation-based initial fields, which is forced by rising CO_2 and climatological or repeated year atmospheric forcing. In the final transient simulation, which forms the basis for our analyses, the model is run with evolving atmospheric pCO_2 and interannually varying climate forcing from typically 1948 or 1958 (when interannual varying reanalysis fields are available) until 2018. The length of the two spin-up phases and of the transient simulation, the atmospheric pCO_2 time history, and the surface boundary conditions used can all vary from one model to the next. Some, but not all, GOBMs represent the net land-sea carbon fluxes ($f_{land\text{-}sea}$) with carbon input from rivers and burial of carbon in marine sediments. For all simulations, model output is provided from 1980 to 2018 at monthly resolution for surface data such as air-sea CO_2 fluxes, and at annual resolution for interior data such as DIC concentrations, after re-gridding the model output to the regular RECCAP2 grid ($1° \times 1°$ horizontal resolution and fixed depth levels). See Table S1 in Supporting Information S1 for further details.

Each modeling group performed at least two and up to four model simulations over the period 1980–2018, where the influence of surface forcing and atmospheric CO_2 are analyzed either in isolation or combination. These simulations are labeled A–D (Table 1). In Simulation A (performed by all models), both the atmospheric CO_2 concentration and surface forcing are varied throughout the simulation period, providing an estimate of the oceanic CO_2 sink under time-evolving climatic conditions and atmospheric CO_2. These simulations capture the net sea-air CO_2 flux ($f_{sea\text{-}air}$) and transport components discussed in Section 2.2, although most models do not fully represent the net land-sea carbon fluxes (Table 1).

In Simulation B (performed by all models), the atmospheric CO_2 concentration and surface forcing are held to a constant climatological seasonal cycle throughout the simulation period. If this simulation were fully spun up under preindustrial conditions, then this simulation would capture only the steady-state preindustrial fluxes ($f_{sea\text{-}air,ss}$) and transports ($J_{DIC,ss}$) as discussed in Section 2.2. However, the models are often incompletely spun up, or they are spun up under a higher atmospheric pCO_2 than preindustrial levels (Table S1 in Supporting Information S1), such that the sea-air CO_2 fluxes and transports are not the same as they would be in a preindustrial steady-state. The difference between the carbon fluxes and transports in simulation B, and those that would be simulated by the models in a preindustrial steady-state, are considered model biases and drifts (Hauck et al., 2020), and denoted by $f_{bias+drift}$ and $J_{DIC,\,bias+drift}$, respectively (Table 1). The bias is the component of the difference that is constant in time, while the drift is the component that is changing in time (Hauck et al., 2020). These biases and drifts are not "real" in the sense that they are not caused by a physical phenomenon and would not exist if the model were in equilibrium with the climate forcing and pCO_2 used to initialize the model (Séférian et al., 2016). The effect of model biases and drifts on the modeled sea-air CO_2 fluxes and transports can be removed by subtracting the results of Simulation B from the other model simulations (note that this also removes the preindustrial steady-state fluxes and transports, which is important for local analyses, but much less so for global integral analyses, since these preindustrial steady-state fluxes and transports sum to near zero globally).

In Simulation C (performed by 11 out of 12 models) the atmospheric CO_2 concentration is varied following the observed time history throughout the simulation, while the surface forcing is held to the same constant climatological seasonal cycle as in Simulation B, providing an estimate of the oceanic CO_2 sink that is driven solely by increasing atmospheric CO_2 concentrations without any climate-driven variability. This simulation captures the anthropogenic CO_2-driven fluxes and transports ($f_{ant,CO2}$ and $J_{DIC,ant,CO2}$), in addition to the components captured by Simulation B (Table 1).

In Simulation D (performed by 11 out of 12 models), the atmospheric CO_2 concentration is held constant while the surface forcing is varied over time using the same atmospheric forcing as in Simulation A, providing an estimate of the variability in the oceanic CO_2 sink that is due to climate variability in the absence of any changes in atmospheric CO_2. This simulation captures the steady-state sea-air CO_2 fluxes and transports of DIC, and the climate-driven natural CO_2 fluxes and transports, $f_{\text{nat, climate}}$ and $J_{\text{DIC,nat,climate}}$ (Table 1).

2.3.2. Data Assimilation Models

In addition to the 12 GOBMs, we also use three different data assimilation models. Here, we use the term "data assimilation" to refer to models that assimilate oceanographic tracer observations in order to improve their representation of ocean processes. In the "assimilation" phase, the circulation or biogeochemistry of these models is adjusted in order to improve the fit of the model to the observations. Two of these data assimilation models are different versions of the OCIM (DeVries, 2014, 2022). The OCIM assimilates observations of potential temperature, salinity, radiocarbon, and CFCs, as well as estimates of sea-surface height and air-sea heat and freshwater fluxes, into a steady-state ocean circulation model. This ocean circulation model is then used as the physical transport model in an abiotic ocean carbon cycle model coupled with rising atmospheric CO_2 levels to estimate air-sea CO_2 fluxes over the period 1780–2018. No data assimilation takes place during this phase. The two OCIM versions, OCIMv2014 (DeVries, 2014) and OCIMv2021 (DeVries, 2022), differ in that OCIMv2021 has a higher vertical resolution, a shallower surface mixed layer, includes a tidal mixing scheme, and assimilates δ^3He observations in addition to the other tracers listed above (Holzer et al., 2021). OCIMv2014 performed simulations A and B only and used an annual time-step for the carbon cycle model, while OCIMv2021 performed simulations A, B, and C and used a monthly time-step for the carbon cycle model. Because of the constant circulation of the OCIM models, their simulation A does not include a representation of the circulation-driven CO_2 fluxes and transports that the GOBMs do. In the case of OCIM-v2021, simulation A includes variable sea surface temperatures and gas transfer velocities, while in OCIM-v2014 these are held constant, making simulation A equivalent to simulation C in that version. Because these simulations do not include biology, the model captures only abiotic processes that affect the ocean carbon sink. Therefore, the regional distribution of air-sea CO_2 fluxes and carbon transports in the OCIM differ from those in the GOBMs and ECCO-Darwin model (see below) that do resolve biologically driven carbon fluxes. Because of these issues, the OCIM is primarily used to estimate the anthropogenic component of the air-sea CO_2 fluxes and DIC accumulation.

The other assimilation model used here is the ECCO-Darwin model (Carroll et al., 2020, 2022). This model features an ocean biogeochemistry and ecology model (Darwin) (Dutkiewicz et al., 2015) coupled to the ECCO data-assimilated physical circulation model (Forget et al., 2015; Zhang et al., 2018). The ECCO circulation is time-varying and assimilates potential temperature, salinity, sea surface height, air-sea heat and freshwater fluxes from 1992 to 2018. The biogeochemistry optimization adjusts initial conditions and several parameters of the Darwin model to match time-varying observations of pCO_2, DIC, alkalinity, nutrients and oxygen in the ocean from 1992 to 2018. This assimilation period coincides with Simulation A in this model. Like the GOBMs, this simulation A captures the effects of both climate-driven and CO_2-driven fluxes, but unlike the GOBMs there could additionally be drifts introduced by changes to the model's biogeochemical parameters during the assimilation. Simulations B-D are not performed with this model. Because there is no simulation B, and because of the incomplete spin-up and potential for model drifts in the first few years of the assimilation period, only the time period from 2001 to 2018 is used in our analysis. Because simulations C and D are lacking, it is not possible to separate the anthropogenic and natural carbon cycling in this model like it is with the GOBMs.

In the analysis that follows, results from the assimilation models are presented separately from those of the GOBMs. Additionally, the OCIM results are presented separately from the ECCO-Darwin results due to the very different nature of the two assimilation models.

2.3.3. Surface Ocean pCO_2-Observation Products

We use a variety of products that estimate global air-sea CO_2 fluxes based on sea surface pCO_2 observations. The bulk of the seawater pCO_2 observations used by these approaches are contained in the Surface Ocean CO_2 Atlas (SOCAT) data product (Bakker et al., 2016). SOCAT compiles and quality-controls pCO_2 observations from research cruises, ships of opportunity, moorings (e.g., Sutton et al., 2019), and autonomous platforms (e.g., Nickford et al., 2022). Various approaches have been devised to fill the gaps in this database to create near-global and temporally complete maps of seawater pCO_2 for nearly the entire open ocean and, for RECCAP2, at monthly

resolution from roughly the mid-1980s to 2018, although some recent approaches have extended these estimates back to before 1960 (Bennington et al., 2022; Rödenbeck et al., 2022). These gap-filling (or interpolation) techniques include statistical (Rödenbeck et al., 2013), multi-linear regression (Iida et al., 2021), and various machine learning algorithms (Chau et al., 2022; Denvil-Sommer et al., 2019; Gloege et al., 2022; Gregor et al., 2019; Landschützer et al., 2014; Zeng et al., 2022). The interpolation step in these models is significant because on average only 1%–2% of the 1° × 1° grid cells at any given month are occupied by actual seawater pCO_2 observations, and the remaining 98%–99% must be filled in by the algorithms (Fay et al., 2021; Rödenbeck et al., 2015). In all, there are 11 different pCO_2-observation products in RECCAP2 that use different approaches to fill gaps in the observational record (Table S2 in Supporting Information S1).

After the reconstruction of surface seawater pCO_2, each group uses a bulk formula to compute the net sea-air CO_2 flux at a monthly resolution using

$$f_{\text{sea-air}} = K_w \times (1 - f_{\text{ice}}) \times K_0 \times (pCO_{2,\text{sw}} - pCO_{2,\text{air}}) \quad (12)$$

where K_w is the wind-speed dependent monthly averaged gas transfer velocity, $(1 - f_{\text{ice}})$ is the percentage of open water in the pixel (sea ice is assumed to be impervious to gas transfer), K_0 is the CO_2 solubility in seawater, and $pCO_{2\text{sw}}$ and $pCO_{2\text{air}}$ are the seawater and air pCO_2, nominally at 5-m depth and 10-m height. Table S2 in Supporting Information S1 provides detailed information on the products used in the computation of the gas transfer velocity, solubility, and atmospheric pCO_2 for each data product.

We note that Equation 12 is also used in the GOBMs to compute the sea-air CO_2 flux, but using the seawater pCO_2 simulated in the model in place of the seawater pCO_2 reconstructed from observations. When comparing the results of the pCO_2 products to those of the GOBMs, it should be considered that the pCO_2 products resolve all of the components of the net air-sea CO_2 flux discussed in Section 2.2 (Table 1). This is because the pCO_2 products are derived from real-world observations and these observations implicitly capture all of the mechanisms that can influence seawater pCO_2. There are no equivalent biases or drifts in the sea-air CO_2 fluxes calculated by the pCO_2 products in the sense that they are not affected by a "spin-up" period or by the need to be in equilibrium with a preindustrial pCO_2. However, there are structural biases in these products, just as there are in the GOBMs, that can affect their ability to accurately reproduce the air-sea CO_2 fluxes. These structural biases are discussed in Section 4.2.

Two of the pCO_2 products differ fundamentally from the core products, and thus are reported separately in the analysis below. One of these is the UOEX product (Watson et al., 2020), which deviates from the others when computing $F_{\text{sea-air}}$ by adjusting pCO_2 observations to account for the cooler skin temperatures of the surface ocean, and adjusting for temperature biases between measurement temperature and sea-surface temperature. These adjustments lead to larger CO_2 fluxes into the ocean. The other is a climatology of sea-air CO_2 fluxes constructed from pCO_2 observations corrected to the year 2010. This climatology follows the methodology used by Takahashi et al. (2009) to normalize all seawater pCO_2 observations collected from 1985 to 2018 to the year 2010. We refer to this product as the "Takahashi update" and consider the fluxes to represent a quasi-decadal average centered on the year 2010.

2.3.4. Interior DIC Products

An extended multiple linear regression approach applied to the C* tracer (eMLR-C*) estimates the increase in anthropogenic DIC in the ocean from 1994 to 2007 (Clement & Gruber, 2018; Gruber et al., 2019a, 2019b). This product uses a multiple linear regression approach with independent variables, such as temperature, salinity, oxygen, and nutrients to capture the variability in C*, with the C* fields derived from global ocean interior observations contained in GLODAPv2 (Olsen et al., 2016). The eMLR-C* estimates include the anthropogenic CO_2-driven as well as the climate-driven anthropogenic DIC accumulation (Gruber et al., 2019a, 2019b; Table 1). This product provides near-global coverage, but is missing data in some marginal seas, and the analysis is cut off below 3,000 m where the anthropogenic DIC signal-to-uncertainty ratio is low. A recent update of the eMLR(C*) results by Müller et al. (2023) resolves decadal trends in the anthropogenic carbon accumulation from 1994 to 2014, but was published after the completion of this study and could thus not be considered here.

2.4. Uncertainties

Unless otherwise stated, uncertainties are derived from the ensemble standard deviation for the GOBMs, pCO_2 products, and OCIM. For most calculations, we use an ensemble of 12 different GOBMs (Table S1 in Supporting Information S1) and nine different pCO_2 products (Table S2 in Supporting Information S1), excluding the UOEX

and Takahashi update products, which are reported separately. For the OCIM, we have only two different versions that are used to assess uncertainties. The ECCO-Darwin, UOEX, Takahashi update, and eMLR-C* are standalone products for which there is no ensemble that can be used to assess uncertainties. For these, we use published uncertainty estimates where available, although for some quantities there are no published uncertainty estimates. For quantities derived by combining two or more different data classes (e.g., GOBMs and pCO_2 products) we use all possible combinations to compute the standard deviation, and refer to the result as the cross-ensemble standard deviation. While the ensemble standard deviation is one measure of variability within or across different products, it does not adequately capture all of the uncertainty due to structural errors and biases in the models and observation-based products. These structural biases, which are more difficult to assess but likely dominate the total uncertainty, are discussed at more length in Section 4.2.

3. Results

This section shows results of the ocean carbon sink estimated by RECCAP2 products for sea-air CO_2 fluxes (Section 3.1) and changes in ocean interior DIC (Section 3.2). Subsections provide discussion of these estimates in light of previous estimates and current knowledge, as well as investigation of the processes responsible for trends and variability of the ocean carbon sink.

3.1. Sea-Air CO_2 fluxes

3.1.1. Results From RECCAP2 Models and Observation-Based Products

Figure 1 illustrates the spatial distribution of sea-air CO_2 fluxes averaged over the RECCAP2 period (1985–2018) from the ensemble of GOBMs and the core pCO_2 products. In both product classes, the strongest outgassing of CO_2 occurs at the equator, especially in the Eastern Tropical Pacific, driven by a convergence of DIC due to upwelling of waters that have accumulated large amounts of respired DIC, and by surface warming (Feely et al., 2006). Outgassing of CO_2 also occurs in other upwelling regions such as the eastern boundary currents of the North and South Pacific, the Mauritanian and Benguela upwelling off the coast of North and South Africa, the seasonal upwelling zone of the Arabian Peninsula, and along the polar front in the Southern Ocean (~50°S). Throughout most of the remaining mid- to high-latitude open ocean the average sea-air CO_2 flux is directed into the ocean. This net uptake is due partly to the removal of DIC by biological uptake, and partly to the cooling of water masses during poleward transport, particularly in the western boundary current regions. In all regions the uptake of anthropogenic CO_2 modifies the fluxes by reducing outgassing in source regions and enhancing ingassing in sink regions (see Section 3.1.2).

The mean area-normalized net sea-air CO_2 flux is -0.48 ± 0.06 mol C m^{-2} yr^{-1} in the GOBMs and -0.41 ± 0.07 mol C m^{-2} yr^{-1} in the pCO_2 products (1985–2018). The bias and drift assessed by Simulation B averages -0.02 ± 0.06 mol C m^{-2} yr^{-1}, which if corrected for would bring the mean sea-air CO_2 flux in the GOBMs to -0.46 ± 0.06 mol C m^{-2} yr^{-1}. Thus, the global mean sea-air CO_2 fluxes in the GOBMs and pCO_2 products agree within their ensemble standard deviations. This agreement is somewhat surprising given that most GOBMs do not represent the outgassing of terrestrially derived CO_2, which has been estimated at between 0.2 and 1.2 PgC/yr globally or 0.05–0.28 mol C m^{-2} yr^{-1} (Jacobson et al., 2007; Kwon et al., 2021; Lacroix et al., 2020; Resplandy et al., 2018), with a recent best estimate of 0.65 ± 0.3 PgC/yr or 0.15 ± 0.07 mol C m^{-2} yr^{-1} (Regnier et al., 2022).

Despite their broad similarities, the difference between the net sea-air CO_2 flux in the GOBMs and the pCO_2 products is significant in some regions (Figure 1c). One prominent difference is enhanced equatorial outgassing in the pCO_2 products relative to the GOBMs. The mean difference between the pCO_2 products and GOBMs in the equatorial Pacific and Indian Oceans reaches up to 1 mol C m^{-2} yr^{-1}. Other regions where the difference between the GOBMs and pCO_2 products exceeds the cross-ensemble standard deviation include the western boundaries of the North Atlantic and North Pacific and the extension systems of the western boundary currents, where the pCO_2 products take up less CO_2 than the GOBMs (Figure 1c). This could be related to model biases, as the GOBMs tend to underestimate wintertime pCO_2 in the western boundary currents, leading to too strong CO_2 uptake in this region (Roobaert et al., 2022). In contrast, the pCO_2 products suggest stronger oceanic CO_2 uptake than the GOBMs in the North Atlantic subtropical gyre, the central to eastern North Pacific, and the eastern South Pacific near the coast of South America. In the Southern Ocean, the pCO_2 products have more outgassing of CO_2 south of the polar front and stronger uptake of CO_2 to the north of the polar front relative to the GOBMs (Figure 1c).

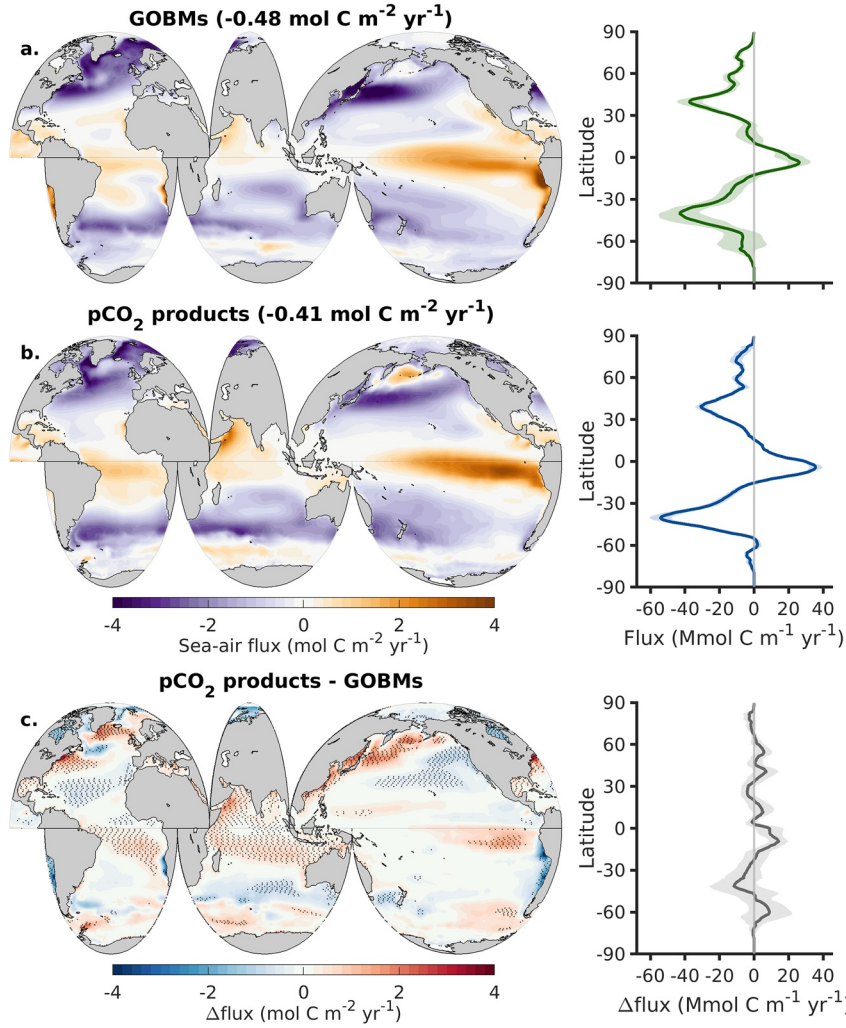

Figure 1. Global mean sea-air CO_2 flux for 1985–2018 for the (top panels) mean of the global ocean biogeochemical models (GOBMs) (simulation A), and (middle panels) mean of the core pCO_2 products (excluding the UOEX and Takahashi update products). The global average sea-air CO_2 flux is given in the title of each figure. Zonally integrated sea-air CO_2 fluxes are shown in the right-hand panels in each figure, with shading representing the ensemble standard deviation. (bottom panels) The difference between the sea-air CO_2 flux in the pCO_2 products and the GOBMs. Stippling indicates regions where the mean sea-air CO_2 flux difference is greater than the cross-ensemble standard deviation. Zonally integrated differences in sea-air CO_2 fluxes are shown in the right-hand panel, with shading representing the cross-ensemble standard deviation. See Figure S1 in Supporting Information S1 for the sea-air CO_2 fluxes in these products over the 2005–2015 period, and Figure S2 in Supporting Information S1 for 2005–2015 sea-air fluxes in the OCIM, ECCO-Darwin, and UOEX products.

Globally integrated net sea-air CO_2 fluxes ($F_{\text{sea-air}}$) for the period 1985–2018 are shown in Figure 2a for all the models and pCO_2 products. For the models (except ECCO-Darwin), simulation A–B is shown in order to remove model drifts and biases, which average -0.11 ± 0.18 PgC yr^{-1} in the GOBMs (Table S1 in Supporting Information S1). This also removes the $F_{\text{land-sea,ss}}$ component of sea-air CO_2 flux that is due to the net land-sea carbon fluxes that must be balanced by sea-air CO_2 fluxes at steady-state (Equation 4), although this is small in most GOBMs (median value of 0 PgC/yr; Table S1 in Supporting Information S1). For ECCO-Darwin, simulation B was not available, and the influence of model drifts is not known. However, it is known that the ECCO-Darwin model has a large unbalanced sink of carbon due to seafloor burial, resulting in a $F_{\text{land-sea}}$ of -1.3 PgC/yr. Because of this, the ECCO-Darwin sea-air fluxes are much lower (more negative) than they would be if $F_{\text{land-sea}}$ were zero, as it is in most of the GOBMs and OCIM. For these reasons, the ECCO-Darwin results cannot be directly compared to the GOBM and OCIM results. For completeness we still show the ECCO-Darwin results in Figure 2, but caution should be taken when interpreting their results.

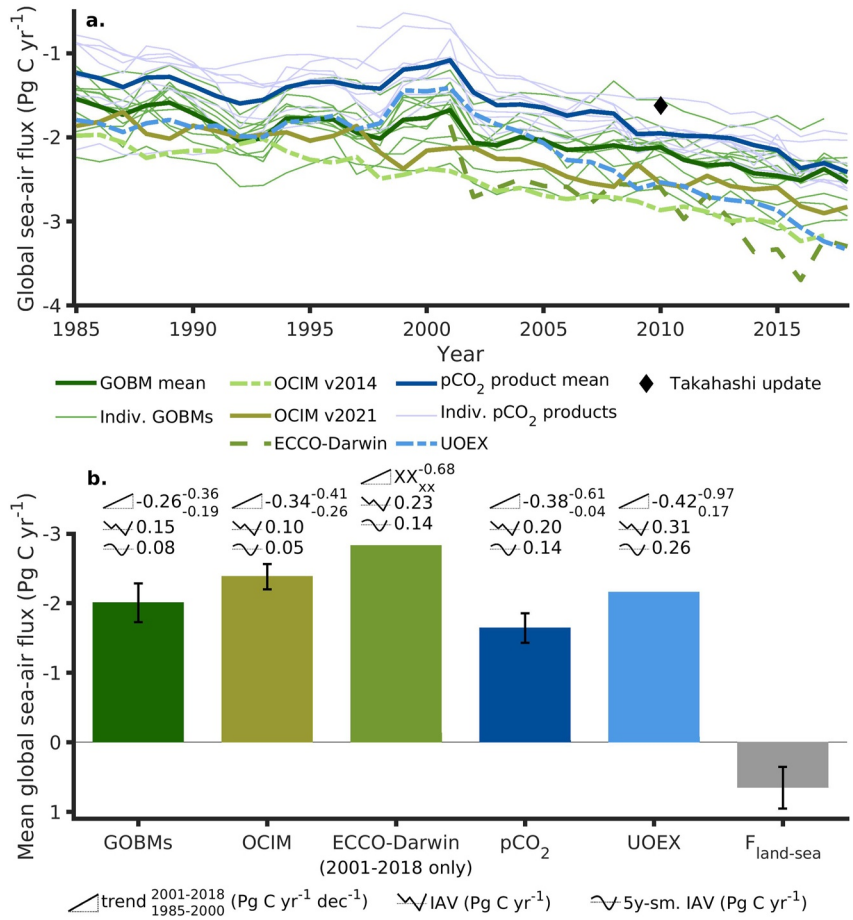

Figure 2. Comparison of different estimates of the ocean CO_2 sink from 1985 to 2018. (a) Globally integrated sea-air CO_2 fluxes from models (shades of green, with model drifts and land-sea fluxes removed, except for ECCO-Darwin) and pCO_2 products (shades of blue). The updated Takahashi climatology is shown by the black diamond in 2010. (b) Summary statistics for the models and pCO_2 products shown in panel (a). Bar heights represent the mean globally integrated sea-air CO_2 flux for the period 1985–2018. Error bars indicate the ensemble standard deviation. Numbers above each graph represent the trend over 1985–2018 (upward trending line, top), with superscripts and subscripts the trend for 2001–2018 and 1985–2000, respectively; the magnitude of the interannual variability (IAV, squiggly line, middle) and the 5-years smoothed IAV (smooth squiggle, bottom). Statistics for the ECCO-Darwin model are only given for the 2001–2018 period. The gray bar is an estimate of the net land-sea carbon flux, $F_{\text{land-sea}}$, for the contemporary ocean (Regnier et al., 2022).

All products show a net uptake of CO_2 by the ocean throughout the RECCAP2 period, with the uptake increasing over time. For the GOBMs, the mean globally integrated sea-air CO_2 flux over the RECCAP2 period is -2.0 ± 0.3 PgC yr^{-1} (Figure 2b) with a maximum of -1.5 and a minimum of -2.6 PgC yr^{-1} over the ensemble of GOBMs. The OCIM exhibits sea-air CO_2 fluxes on the lower (more uptake) end of this range, with an average global sea-air flux of -2.4 ± 0.2 PgC yr^{-1} from 1985 to 2018. Sea-air CO_2 fluxes reconstructed by the pCO_2 products are generally less negative (less CO_2 uptake) than those predicted by the models. The mean sea-air CO_2 flux from the core pCO_2 products (excluding UOEX and Takahashi update) is -1.6 ± 0.2 PgC yr^{-1} (min of -2.0 and max of -1.3). The difference between the global sea-air CO_2 flux of the pCO_2 products and that of the GOBMs is 0.4 ± 0.3 PgC yr^{-1}, while the difference between the pCO_2 products and the OCIM is 0.7 ± 0.3 PgC yr^{-1}.

Globally integrated sea-air CO_2 fluxes estimated by the pCO_2 products are systematically less negative than those predicted by the GOBMs and OCIM. Several factors could help explain this. First, the global sea-air CO_2 flux from the GOBMs and OCIM reported in Figure 2 do not include fluxes that result from the net land-sea carbon flux ($F_{\text{land-sea}}$), thus the model results represent only $F_{\text{ant,CO2}}$ and F_{climate} (see Equation 8). The current best estimate of $F_{\text{land-sea}}$ is 0.65 ± 0.3 PgC yr^{-1} (Regnier et al., 2022), as shown by the gray bar in Figure 2b. If this flux were added to the GOBM and OCIM estimates of sea-air CO_2 flux, it would yield a net sea-air CO_2

flux of -1.4 ± 0.4 PgC yr^{-1} in the GOBMs, and -1.7 ± 0.4 PgC yr^{-1} in the OCIM. Second, some of the pCO_2 products do not cover the entire ocean surface, but are missing data in polar regions and marginal seas (Table S2 in Supporting Information S1). If the mean sea-air CO_2 flux of -0.41 mol m^{-2} yr^{-1} from the pCO_2 products is scaled to the global ocean surface area of 3.6×10^{14} m^2, this yields a slightly more negative sea-air CO_2 flux of -1.8 ± 0.3 PgC yr^{-1}. This simple scaling yields results that are similar to those based on explicit reconstruction of coastal sea-air CO_2 fluxes (Fay et al., 2021).

The models and pCO_2 products also differ in the temporal variability of the globally integrated sea-air CO_2 flux (Figure 2b). The magnitude of interannual variability (IAV), which is here defined as the temporal standard deviation of the linearly detrended annual globally integrated sea-air CO_2 fluxes (see DeVries, 2022 for details), ranges from 0.10 PgC yr^{-1} in the OCIM to 0.31 PgC yr^{-1} in the UOEX pCO_2 product (Figure 2b). In general, the pCO_2 products have a greater IAV (mean of 0.20 PgC yr^{-1}) than the GOBMs (mean of 0.15 PgC yr^{-1}) (Figure 2b). The dominant factor leading to year-to-year variability in sea-air CO_2 fluxes is ENSO (Rodenbeck et al., 2015), which strengthens global ocean CO_2 uptake during El Niño phases and weakens during La Niña (Bacastow, 1976; Feely et al., 1999; Ishii et al., 2014; Keeling & Revelle, 1985; Liao et al., 2020; McKinley et al., 2004). The influence of short-term climate modes such as ENSO can be filtered out by taking the 5-years running average of the IAV, which better captures the decadal timescales of variability. The 5-years smoothed variability of the pCO_2 products is twice as large as that of the GOBMs, and three times as large as that in the OCIM (Figure 2b).

Large decadal variability in the pCO_2 products is partly driven by a strong shift of the trend in global sea-air CO_2 flux around the year 2000. From 1985 to 2000, the global sea-air CO_2 flux in the pCO_2 products trended nearly flat, at a rate of -0.04 ± 0.29 PgC yr^{-1} decade^{-1} (Figure 2b). After 2000, the pCO_2 products trend toward much stronger uptake, at a rate of -0.61 ± 0.12 PgC yr^{-1} decade^{-1} from 2001 to 2018 (similar to the trend of -0.68 PgC yr^{-1} decade^{-1} in the ECCO-Darwin model during that period). By contrast, the GOBMs show a weak strengthening trend from 1985 to 2000 at a rate of -0.19 ± 0.07 PgC yr^{-1} decade^{-1}, and a more muted transition to stronger uptake after 2000, with a trend of -0.34 ± 0.06 PgC yr^{-1} decade^{-1} from 2001 to 2018.

3.1.2. Mechanisms Contributing to Sea-Air CO_2 Fluxes in RECCAP2 Models

Model simulations for RECCAP2 were designed to isolate the mechanisms responsible for the magnitude and variability of sea-air CO_2 fluxes (Table 1). Here we decompose the net sea-air CO_2 fluxes in models and pCO_2 products into anthropogenic and natural components, and investigate the roles of climate variability and atmospheric CO_2 in controlling the global sea-air CO_2 fluxes during the RECCAP2 period.

At a local scale, the net sea-air CO_2 flux ($f_{\text{sea-air}}$; Figure 1) is composed of the preindustrial steady-state sea-air fluxes ($f_{\text{sea-air,ss}}$), anthropogenic CO_2-driven uptake flux ($f_{\text{ant,CO2}}$), and the climate-driven CO_2 flux (f_{climate}) (see Equations 9 and 10). These fluxes can be decomposed in the GOBMs to determine the processes responsible for the spatial distribution of sea-air CO_2 fluxes averaged over 1985–2018 (Figure 3). Simulation B in the GOBMs captures $f_{\text{sea-air,ss}}$ as well as biases and drifts that may be due to incomplete model spin-up ($f_{\text{bias+drift}}$). The spatial pattern of sea-air CO_2 flux in Simulation B (Figure 3a) bears a strong resemblance to the net air-sea CO_2 flux from Simulation A (Figure 1a), indicating that the natural steady-state sea-air CO_2 flux is the dominant component of the local net sea-air flux. The global mean of these fluxes is a small net uptake of -0.02 ± 0.06 molC m^{-2} yr^{-1}. This small negative flux is due to incomplete spinup of these models leading to model drift (Séférian et al., 2016), and in the case of some models a negative net land-sea carbon flux ($f_{\text{land-sea}}$) due to an excess of carbon burial over river inputs (Table S1 in Supporting Information S1).

The second most important component of $f_{\text{sea-air}}$ is $f_{\text{ant,CO2}}$ (Figure 3b). In the GOBMs and OCIM this component is found by the difference between simulations C and B. The sign of $f_{\text{ant,CO2}}$ is everywhere negative, indicating CO_2 uptake by the ocean, with the highest uptake rates in the North Atlantic, Southern Ocean, western boundary currents, and the equatorward flanks of the subtropical gyres (see also Mikaloff-Fletcher et al., 2006). These regions experience the re-emergence of waters whose anthropogenic carbon content is not in equilibrium with the atmosphere, and have strong surface winds that promote fast gas exchange rates (Caldeira & Duffy, 2000; Ishii et al., 2020; Ridge & McKinley, 2020; Sarmiento et al., 1992; Toyama et al., 2017).

The climate-driven sea-air CO_2 flux can be further decomposed into the climate-driven natural flux, $f_{\text{nat, climate}}$, and the climate-driven anthropogenic flux, $f_{\text{nat, climate}}$ (Figures 3c and 3d). $f_{\text{nat, climate}}$ is found by the difference of sea-air fluxes in simulation D and simulation B, and $f_{\text{ant, climate}}$ is found by the difference between the total anthropogenic effect including climate variability (simulation A–D), and the CO_2-only anthropogenic effect (simulation

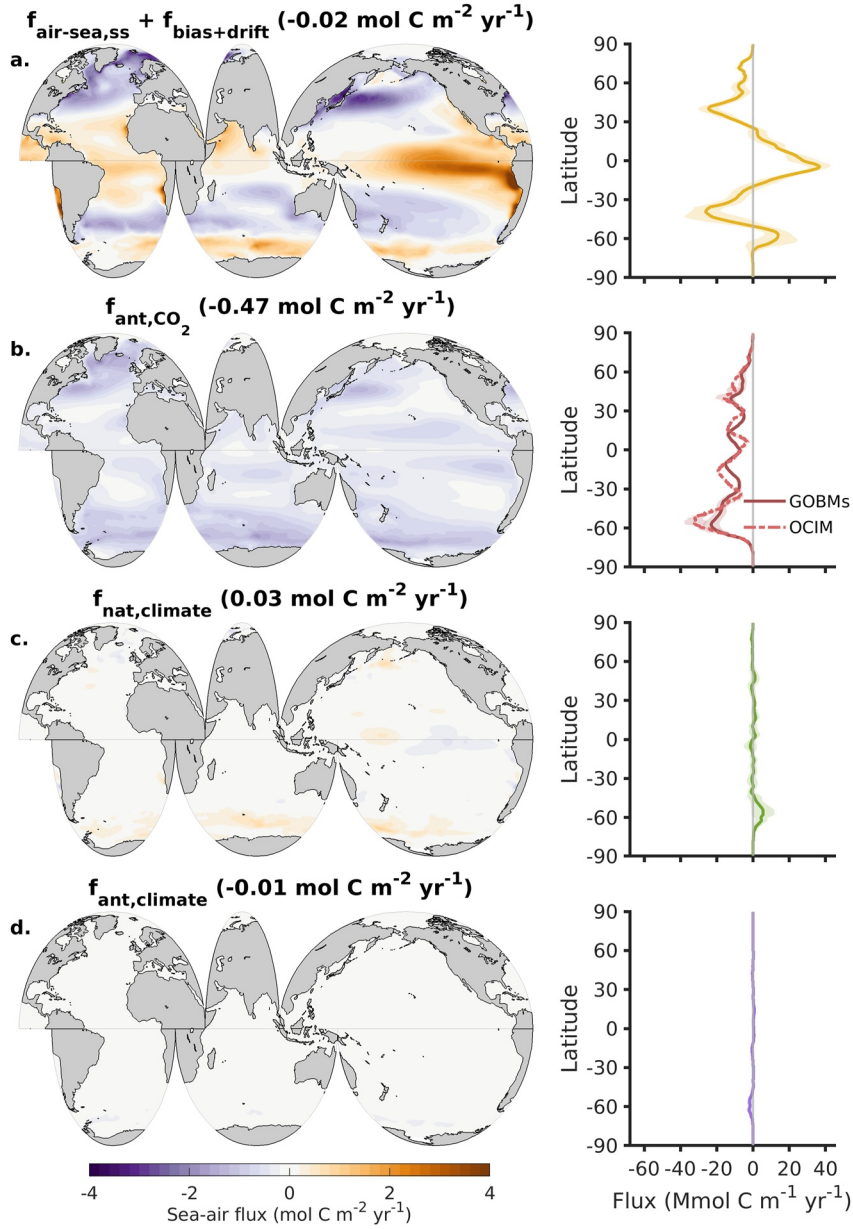

Figure 3. Spatial distribution of sea-air CO_2 flux components in the global ocean biogeochemical models (GOBMs) for the period 1985–2018. Compare with the contemporary sea-air CO_2 flux in Figure 1a. (a) The mean sea-air CO_2 flux from simulation B in the GOBMs, which represents the sum of the pre-industrial steady-state fluxes, $f_{sea\text{-}air,ss}$, and any model biases and drifts during this period, $f_{bias+drift}$. (b) Anthropogenic sea-air CO_2 fluxes driven by atmospheric pCO_2 increase with a constant climate. (c) Climate-driven changes in natural sea-air CO_2 fluxes. (d) Climate-driven changes in anthropogenic sea-air CO_2 fluxes. Numbers in parentheses in the plot title indicate the global average sea-air CO_2 flux for each component. Right-hand subplots show the zonal integral of the flux component in the map, with the solid line representing the ensemble mean and the shading one standard deviation of the ensemble. For panel (b) the ocean circulation inverse model (OCIM) results are additionally shown in the zonal integral. Figure S3 in Supporting Information S1 shows the OCIM sea-air anthropogenic CO_2 fluxes for comparison with panel (b).

C–B) (Table 1). In terms of spatial variability, the natural component of $f_{climate}$ is larger than the anthropogenic component (Figures 3c and 3d), with the standard deviation of $f_{nat,\ climate}$ at 0.31 mol C m^{-2} yr^{-1} compared to 0.10 mol C m^{-2} yr^{-1} for $f_{ant,\ climate}$. The climate-driven CO_2 fluxes are strongest in the Southern Ocean, where climate variability has driven a weak net outgassing of natural CO_2 and an even weaker net ingassing of anthropogenic CO_2 (Figures 3c and 3d). The opposing effects of climate variability on natural and anthropogenic

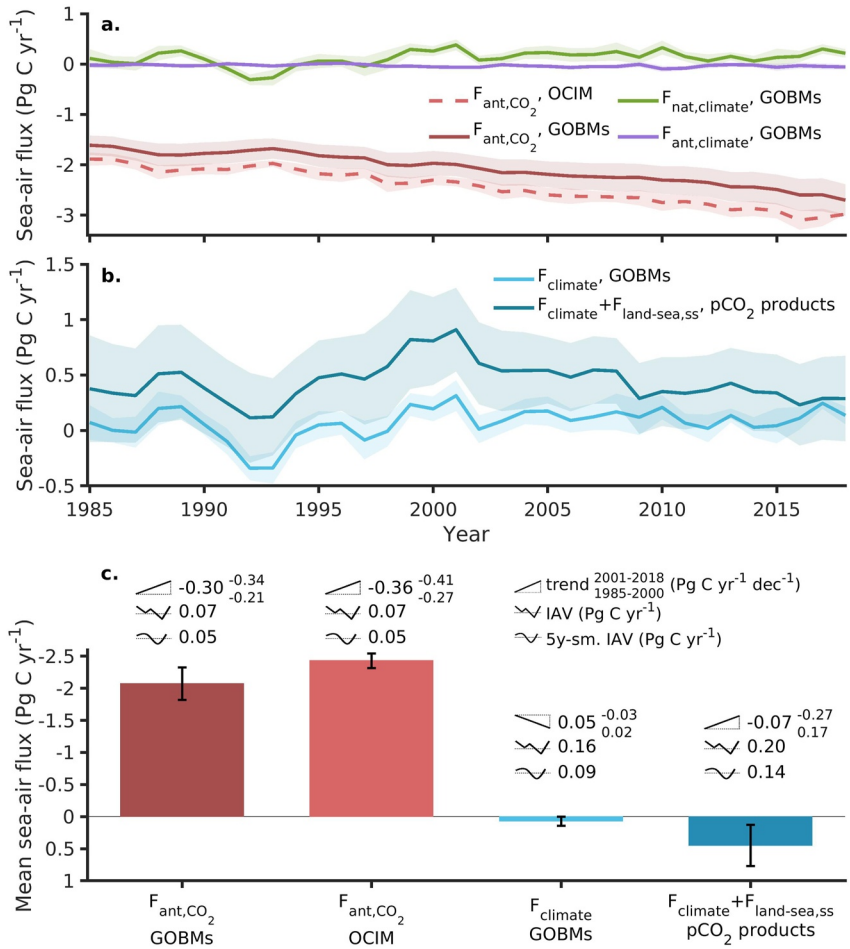

Figure 4. (a) Components of the contemporary net sea-air CO_2 flux in RECCAP2 global ocean biogeochemical models (GOBMs), using simulations A–D to partition fluxes into the anthropogenic CO_2-driven flux ($F_{ant,CO2}$), the climate-driven anthropogenic CO_2 flux ($F_{ant,\ climate}$), and the climate-driven natural CO_2 flux ($F_{nat,\ climate}$). Solid curve is the ensemble mean and shading is the ensemble standard deviation. An estimate of $F_{ant,CO2}$ from the ocean circulation inverse model (OCIM) is also given by the red dashed curve. (b) The climate-driven sea-air CO_2 flux ($F_{climate}$) in the GOBMs, compared with the sum of $F_{climate}$ and the net land-sea carbon flux ($F_{land\text{-}sea,ss}$) in the pCO_2 products. Dark curve is the multi-product mean and light shading is the cross-ensemble standard deviation. (c) Summary statistics (as in Figure 2) for $F_{ant,CO2}$ from the GOBMs (dark red) and the OCIM (light red), $F_{climate}$ from the GOBMs (light blue) and $F_{climate} + F_{land\text{-}sea,ss}$ from the pCO_2 products (dark blue).

air-sea CO_2 fluxes is consistent with previous modeling studies and due to the opposing gradients of natural and anthropogenic DIC in the ocean (e.g., Bernardello et al., 2014; DeVries et al., 2017; Ito et al., 2015). The climate-driven variability of the natural and anthropogenic CO_2 in the Southern Ocean over 1985–2018 is likely due to increased Southern Hemisphere westerly winds, which drive an increase in upwelling along and to the south of the polar front, driving both increased natural CO_2 outgassing and a slight increase in anthropogenic CO_2 uptake (Canadell et al., 2021; Jones et al., 2016; Le Quéré et al., 2007b; Lovenduski et al., 2007). The globally averaged climate-driven sea-air CO_2 fluxes over this period are small, averaging 0.03 mol C m^{-2} yr^{-1} for $f_{nat,\ climate}$ and −0.01 mol C m^{-2} yr^{-1} for $f_{ant,\ climate}$ (Figures 3c and 3d).

The same component separation done for the local sea-air CO_2 flux can be applied to globally integrated flux (Figure 4). This separation reveals that $F_{ant,CO2}$ is by far the dominant component of the globally integrated sea-air CO_2 flux over the RECCAP2 period, while $F_{climate}$ is near zero (Figures 4a and 4c). The mean of $F_{ant,CO2}$ for the RECCAP2 period is -2.1 ± 0.3 PgC yr^{-1} in the GOBMs, and -2.4 ± 0.1 PgC yr^{-1} in the OCIM. The time evolution of $F_{ant,CO2}$ in the OCIM and GOBMs is similar (Figure 4a), although the rate of increase in $F_{ant,CO2}$ is slightly more negative in the OCIM (-0.36 ± 0.02 PgC yr^{-1} $decade^{-1}$ over the full RECCAP2 period) compared to that in the GOBMs (-0.30 ± 0.04 PgC yr^{-1} $decade^{-1}$) (Figure 4c).

While $F_{ant,CO2}$ dominates the magnitude of the globally integrated sea-air CO_2 flux, interannual to decadal variability is predominantly due to $F_{climate}$ (Figures 4a and 4c). The interannual variability of $F_{ant,CO2}$ in both the GOBMs and the OCIM is only 0.07 PgC yr^{-1}, while the 5-years smoothed (decadal) variability is 0.05 PgC yr^{-1} (Figure 4c). A large part of the decadal variability in $F_{ant,CO2}$ is related to low atmospheric CO_2 growth rates in the late 1980s and early 1990s (e.g., McKinley et al., 2020), which caused the ocean anthropogenic CO_2 sink to stagnate or even slightly decline from 1988 to 1993 (Figure 4a). Interannual to decadal variability in $F_{climate}$ is dominated by the natural component, $F_{nat, climate}$ (Figure 4a). In the GOBMs, the interannual variability of $F_{nat, climate}$ is 0.18 ± 0.03 PgC yr^{-1} over 1985–2018, while the IAV of $F_{ant, climate}$ is only 0.04 ± 0.01 PgC yr^{-1}. This difference is due to the fact that there is a much larger concentration of natural DIC than anthropogenic DIC in the ocean, so that climate-driven changes in gas transfer velocity or solubility (e.g., Wanninkhof & Triñanes, 2017), as well as ocean circulation changes (e.g., DeVries et al., 2017), mainly impact the natural air-sea CO_2 fluxes.

$F_{ant,CO2}$ estimated by the OCIM and GOBMs can also be removed from the net sea-air CO_2 fluxes calculated by the pCO_2 products. The difference represents the sum of $F_{climate}$ (both natural and anthropogenic components) and $F_{land\text{-}sea,ss,}$ though with the important caveat that any bias in the $F_{ant,CO2}$ estimate is directly projected on the residual estimate of $F_{climate}$ and $F_{land\text{-}sea,ss}$ (Table 1). Since by definition $F_{land\text{-}sea,ss}$ is constant, the temporal variability in the resulting sea-air CO_2 flux is solely due to $F_{climate}$ (Figure 4b). The interannual variability of $F_{climate}$ in the pCO_2 products is 0.20 ± 0.06 PgC yr^{-1}, which is greater than the IAV of $F_{climate}$ estimated by the GOBMs (0.16 ± 0.03 PgC yr^{-1}). Likewise, the decadal variability of $F_{climate}$ in the pCO_2 products is 0.14 ± 0.05 PgC yr^{-1}, which is about 50% greater than that in the GOBMs (0.09 ± 0.02 PgC yr^{-1}) (Figure 4c). The interannual to decadal variability of $F_{climate}$ predicted by both the GOBMs and the pCO_2 products is about 2–3 times greater than that of $F_{ant,CO2}$ (Figure 4c).

The models and the pCO_2 products agree quite well in the evolution of $F_{climate}$ over the period from 1985 to 2000 (Figure 4b), although the pCO_2 products estimate a larger positive trend of $F_{climate}$ (0.17 ± 0.27 PgC yr^{-1} $decade^{-1}$) than the GOBMs (0.02 ± 0.07 PgC y^{r-1} $decade^{-1}$) over this period (Figure 4c). Climate-driven trends over this time period have been ascribed to changes in upper-ocean overturning circulation (DeVries et al., 2017), particularly in the Southern Ocean (Gruber et al., 2019b; Landschützer et al., 2015), and to changes in ocean temperatures in response to the eruption of Mt. Pinatubo in the early 1990s (McKinley et al., 2020). The $F_{climate}$ trends in the GOBMs and pCO_2 products diverge after 2001. The $F_{climate}$ diagnosed by the GOBMs shows some interannual variability but little trend from 2001 to 2018 (-0.03 ± 0.05 PgC yr^{-1} $decade^{-1}$). Contrastingly, $F_{climate}$ in the pCO_2 products strengthens at a rate of -0.27 ± 0.13 PgC yr^{-1} $decade^{-1}$ from 2001 to 2018 (Figure 3c). This difference in strengthening trends is large enough that the difference between the GOBMs and pCO_2 products, which is commonly attributed to $F_{land\text{-}sea,ss}$ (Friedlingstein et al., 2022), is erased by the year 2018.

The mechanism responsible for the recent negative trend of $F_{climate}$ in the pCO_2 products is not clear, nor is it clear why the strength of the trends differs between pCO_2 products and GOBMs. One possibility is that the pCO_2 products spuriously overestimate recent trends in the ocean CO_2 sink, due to artifacts of the interpolation algorithms when applied to sparse and irregular pCO_2 observations (Denvil-Sommer et al., 2021; Gloege et al., 2021; Hauck et al., 2023). Another possibility is that the pCO_2 products are capturing a real signal that is not present in the models. The pCO_2 products and GOBMs represent climate variability in distinct ways: pCO_2 products tie seawater pCO_2 variability to the observed variability of predictors such as sea surface temperature, mixed layer depth, and chlorophyll concentration (e.g., Gloege et al., 2022), while GOBMs represent climate variability by forcing the model with reanalysis wind stress and surface buoyancy fluxes. If the trends in the pCO_2 products are not spurious, it can be inferred that seawater pCO_2 is increasing less rapidly in the ocean than is predicted by the GOBMs. This could reflect a general tendency of the models to underestimate the climate sensitivity of biogeochemical processes (Andrews et al., 2013; DeVries et al., 2019), or be caused by processes that are not captured in the models, such as a slowdown of the overturning circulation leading to enhanced trapping of DIC in the deep ocean (DeVries et al., 2017). It is also possible that some of the trends seen in the pCO_2 products reflect variability in the input of carbon or alkalinity at the land-sea interface (Drake et al., 2018; Regnier et al., 2013).

3.2. Changes in Interior DIC Storage

3.2.1. Results From RECCAP2 Models and Observation-Based Products

Vertically integrated rates of DIC change are shown in Figure 5 for the RECCAP2 products that provide estimates of interior ocean DIC changes. These include the GOBMs (Figure 5a), the two OCIMs (Figure 5b), the ECCO-Darwin (Figure 5c), and the eMLR-C* product (Figure 5d). Although the different classes of products

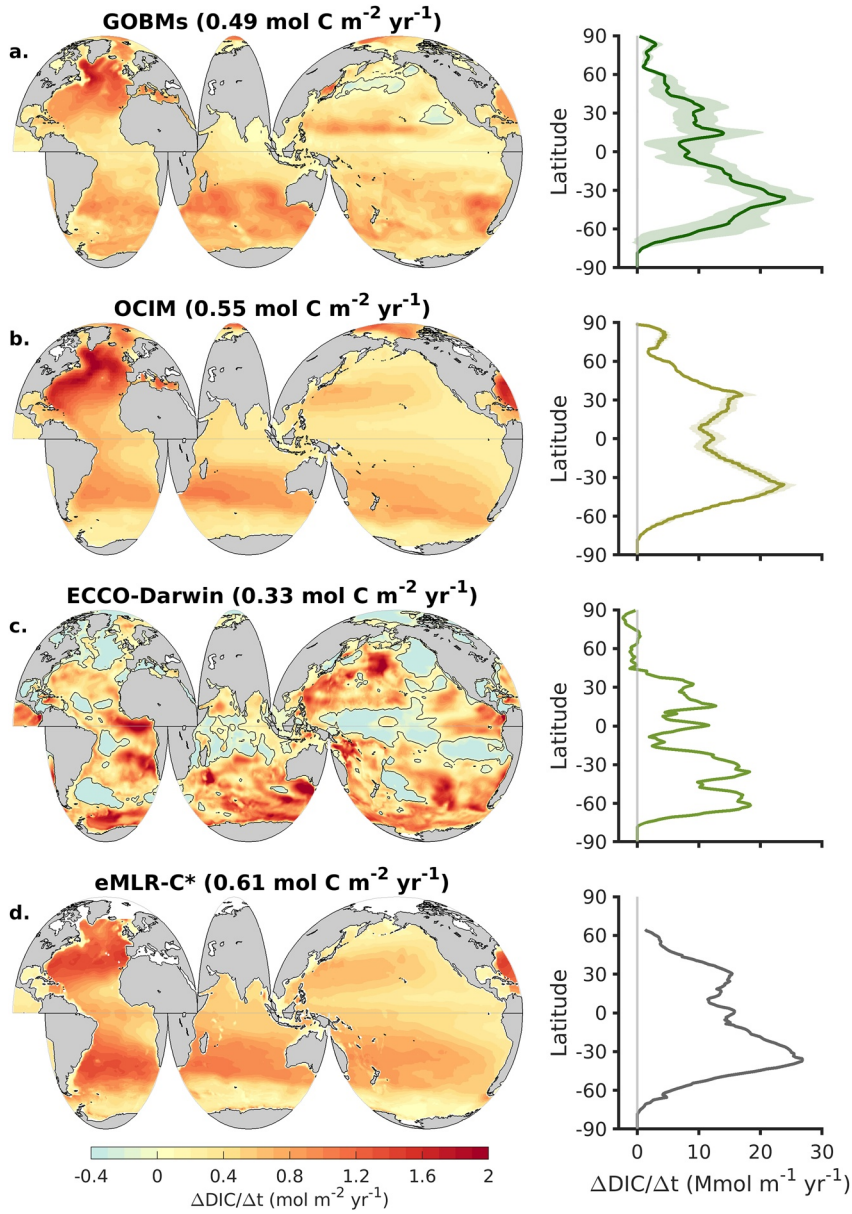

Figure 5. Rate of change in the vertical integral of dissolved inorganic carbon (DIC) storage for (a) the global ocean biogeochemical models (GOBMs) from 1985 to 2018, (b) ocean circulation inverse model from 1985 to 2018, (c) ECCO-Darwin from 2001 to 2018, and (d) eMLR-C* from 1994 to 2007. Simulation A is used for all models. Rates are calculated by subtracting the vertically integrated DIC concentration in 1985 from the vertically integrated DIC concentration in 2018, or the start and end years of each product, and dividing by the number of years elapsed. For GOBMs the mean of 11 models is shown, not including the CCSM. Numbers in parentheses in the title are the areal average rate of change in DIC accumulation over the time period covered by each product. The zero contour is shown as a solid line in all plots. Figure S4 in Supporting Information S1 shows accumulation rates in these products (except ECCO-Darwin) over the 1994–2007 period.

capture different mechanisms that drive variability in DIC concentrations over time (Table 1), here we directly compare the results from each product before using them to separately diagnose the components of DIC variability over time (Section 3.2.2). Because some of the products do not cover the entire RECCAP2 period, we normalize the change in DIC concentration in each product by the time period covered by each product, which makes their magnitudes comparable.

The GOBMs displays an increase in DIC storage throughout most of the ocean over the period 1985–2018 (Figure 5a; Simulation A can be compared to air-sea fluxes reported in Figure 1a). The increase in DIC storage

is most pronounced in the North Atlantic, where vertically integrated rates of DIC accumulation reach up to 2 mol m^{-2} yr^{-1}. DIC accumulation rates of ∼1 mol m^{-2} yr^{-1} are found in the Southern Ocean and Southern Hemisphere subtropics, largest in the Indian sector of the Southern Ocean. Weakest accumulation rates occur in the eastern tropical Pacific, and parts of the North Pacific, where a small loss of DIC over the RECCAP2 period is evident in some areas (Figure 5a). DIC accumulation rates in the OCIM are similar to those of the GOBMs at the large scale, although the OCIM shows greater accumulation of DIC in the western North Atlantic than the GOBMs, and less accumulation in the Antarctic sector of the Southern Ocean (Figure 5b). There are no regions of negative DIC accumulation in the OCIM, because the OCIM primarily captures the accumulation of anthropogenic CO_2 (Table 1), which is positive over the RECCAP2 period due to rising atmospheric CO_2.

The ECCO-Darwin DIC accumulation rates are very different from those in the GOBMs and OCIM (Figure 5c). DIC accumulation is strongest in the Southern Ocean and the western North Pacific, while the subpolar North Atlantic, equatorial West Pacific, and northeastern Pacific are all losing DIC. These large regions of DIC loss are at least partially due to a negative $F_{\text{land-sea}}$ of −1.3 PgC yr^{-1} in the ECCO-Darwin model, which is due to burial of carbon in seafloor sediments that is not balanced by riverine carbon inputs (Table S1 in Supporting Information S1). As a result, the ocean loses DIC over time, counteracting some of the DIC gained by anthropogenic CO_2 uptake. Nonetheless, the ECCO-Darwin shows much greater spatial variability in DIC accumulation rates than the OCIM and GOBMs, and this cannot be attributed to the carbon burial which is relatively constant throughout the ECCO-Darwin simulation. The ECCO-Darwin model is the only model that assimilates ocean DIC observations, and it is designed to provide maximal consistency with the DIC observations. As such, it is possible that the large spatial variability seen in ECCO-Darwin reflects actual climate-driven variability in ocean DIC accumulation. However, it is also possible that some of the patterns seen in ECCO-Darwin are artifacts of the data assimilation process, since changes to biogeochemical model parameters during the assimilation may lead to gradients in DIC that are advected by the mean ocean circulation. Until an in-depth analysis of the mechanisms behind the ECCO-Darwin DIC accumulation patterns can be undertaken, it remains unclear if the patterns seen in Figure 5c represent real variability or assimilation artifacts.

The eMLR-C* product represents the CO_2-driven and climate-driven components of anthropogenic DIC accumulation in the ocean from 1994 to 2007. In this regard the DIC accumulation rate in the eMLR-C* product is most comparable to that in the OCIM, which captures mainly the anthropogenic CO_2-driven change in DIC storage. Like the OCIM, the DIC accumulation rate in the eMLR-C* product is highest in the North Atlantic and displays preferential accumulation in the western North Atlantic, a feature which has been attributed to the flow of anthropogenic CO_2 along the deep western boundary current (Lee et al., 2003; Steinfeldt et al., 2009). Anthropogenic DIC accumulation rates in the Southern Hemisphere midlatitudes are generally larger in the eMLR-C* than those in the OCIM, particularly in the South Atlantic (Figure 5).

The vertical distribution of DIC storage rates reveals further differences among the various RECCAP2 products (Figure 6). In the Atlantic Ocean at intermediate depths (1,000–3,000 m), DIC accumulation in the OCIM exceeds 0.5 mmol m^{-3} yr^{-1} in the subpolar North Atlantic, while the accumulation rate in the South Atlantic is only 0.1 mmol m^{-3} yr^{-1} (Figure 6b), similar to the pattern seen in the GOBMs (Figure 6a). By contrast, the DIC accumulation rate in the eMLR-C* product is roughly 0.2–0.3 mmol m^{-3} yr^{-1} in both the northern and southern hemispheres of the mid-depth Atlantic (Figure 6d). In the deep north Pacific Ocean (>1,000 m depth), the OCIM and eMLR-C* products both estimate very small but positive DIC accumulation rates (<0.1 mmol m^{-3} yr^{-1}), while the GOBMs have slightly negative DIC accumulation rates in this region (Figure 6). Globally, the eMLR-C* has the highest rates of DIC accumulation near the surface (347 Gmol m^{-1} yr^{-1} compared to 317 ± 17 Gmol m^{-1} yr^{-1} in the GOBMs and 307 ± 18 Gmol m^{-1} yr^{-1} in the OCIM) as well as the highest accumulation rates at 3,000 m depth (14 Gmol m^{-1} yr^{-1} in the eMLR-C* compared to 6.9 ± 1.1 Gmol m^{-1} yr^{-1} in the OCIM and 3.2 ± 11 Gmol m^{-1} yr^{-1} in the GOBMs). The eMLR-C* product does not resolve DIC storage below 3,000 m, which averages around 2.5 ± 0.5 Gmol m^{-1} yr^{-1} in the OCIM and 3.7 ± 11.0 Gmol m^{-1} yr^{-1} in the GOBMs. This deep ocean DIC accumulation equates to about 4% and 6% of the globally integrated air-sea CO_2 flux in the OCIM and GOBMs, respectively.

The depth distribution of DIC accumulation in the ECCO-Darwin model is substantially different from all other data sets. Storage rates are high near the surface, but drop to very low or negative values just below the surface mixed layer in the main thermocline, with an average accumulation of −60 Gmol m^{-1} yr^{-1} at 400 m depth. A secondary maximum of DIC accumulation is found at about 1,500 m depth (Figure 6c). Another significant contrast

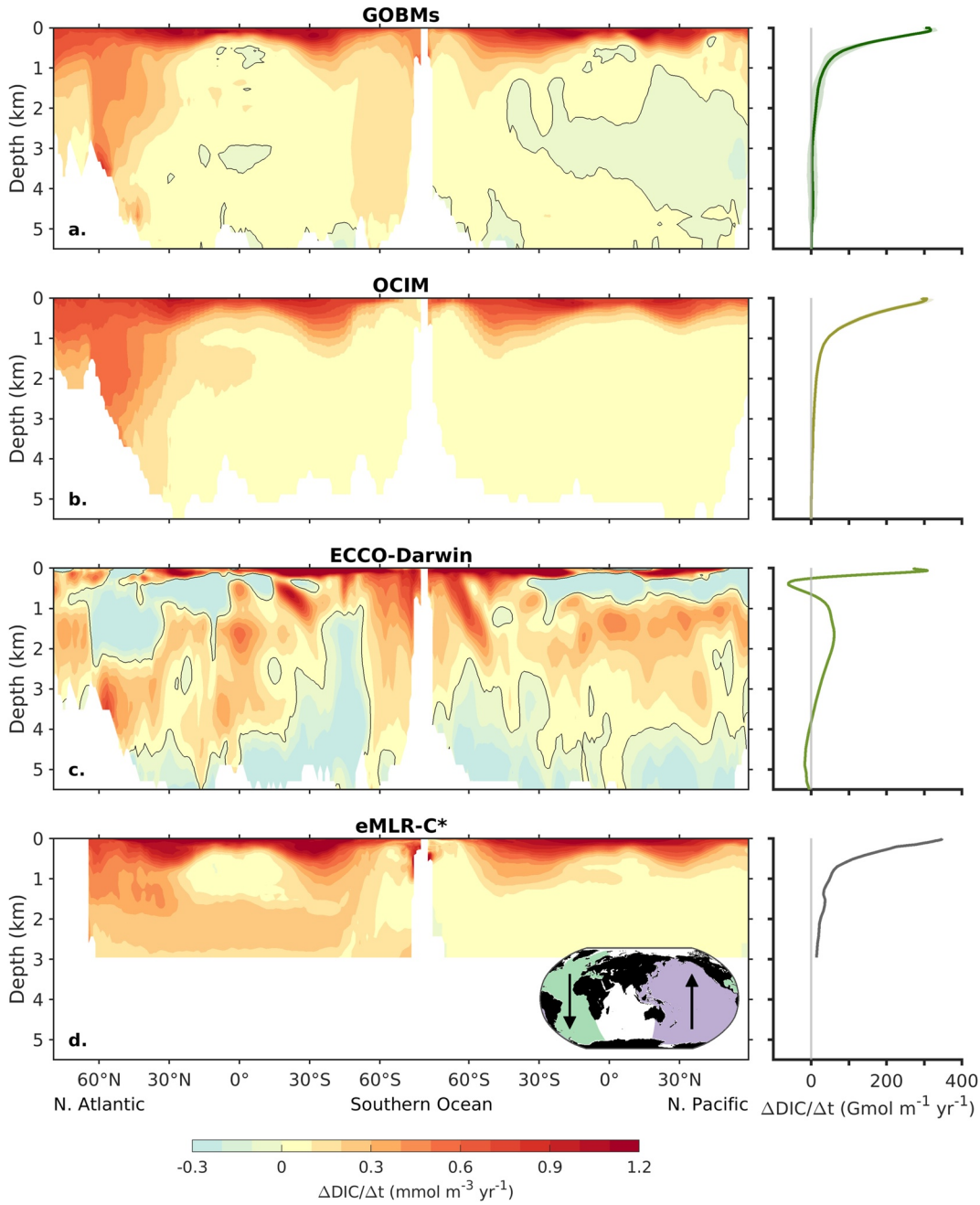

Figure 6. Basin-averaged sections of trends in dissolved inorganic carbon (DIC) storage for (a) global ocean biogeochemical models (GOBMs) over the period 1985–2018, (b) ocean circulation inverse model over the period 1985–2018, (c) ECCO-Darwin over the period 2001–2018, and (d) eMLR-C* over the period 1994–2007. For the GOBMs we show the mean of 11 models (excluding CCSM). Simulation A is used for all models. The inset plot in the bottom panel shows the areas used in the basin average, with the direction of the arrows following the basin averaged plots from the North Atlantic to North Pacific. The zero contour is shown as a solid line in all plots. The right hand plots in each panel show the globally integrated rate of DIC accumulation with depth (shading indicating the ensemble standard deviation), such that the vertical integral of the DIC accumulation rate with depth equals the globally integrated DIC accumulation rate. Figure S5 in Supporting Information S1 shows accumulation rates in these products (except ECCO-Darwin) over the 1994–2007 period.

between the ECCO-Darwin and other products is found in the deep Pacific Ocean where the ECCO-Darwin is accumulating DIC, while the GOBMs are losing DIC and the anthropogenic estimates (OCIM and eMLR-C*) show essentially zero to very little accumulation. The same caveats placed on ECCO-Darwin for Figure 5 apply here—it is still unclear if these patterns represent real-world variability or assimilation artifacts in this model.

3.2.2. Mechanisms Contributing to Changes in DIC Storage in RECCAP2 Products

The differences in DIC storage rates among the RECCAP2 products can be attributed to the different components of DIC storage that are captured by each method (Table 1), as well as structural biases of these products. To more directly compare the products, and to examine the mechanisms driving the DIC accumulation rates, we separated the vertically integrated DIC accumulation rates shown for the GOBMs in Figure 5 into anthropogenic CO_2-driven and climate-driven components of DIC accumulation, and compared these to the same components diagnosed from the OCIM and eMLR-C* methods.

The results show that anthropogenic DIC accounts for the majority of DIC accumulation in the GOBMs (Figure 7a), and the largest single driver of DIC accumulation in the GOBMs is the anthropogenic CO_2-driven component (Figure 7c). The total anthropogenic effect (the sum of the CO_2-driven and climate-driven components) is directly comparable to the eMLR-C* product (Figures 7a and 7b). These two independent estimates are qualitatively and quantitatively similar, with highest anthropogenic DIC accumulation rates in the subpolar North Atlantic and subantarctic Southern Ocean. The eMLR-C* product displays slightly larger anthropogenic DIC accumulation rates in the Southern Hemisphere and subtropical North Atlantic than the GOBMs, while the GOBMs have slightly more anthropogenic DIC accumulation in the Antarctic region of the Southern Ocean south of ~50°S (Figures 7a and 7b). The anthropogenic CO_2-driven DIC accumulation in the GOBMs can be directly compared to that in the OCIM (Figures 7c and 7d), revealing consistent patterns of anthropogenic DIC accumulation. The largest difference between these two products is in the subtropical North Atlantic, where the OCIM predicts nearly twice as rapid DIC accumulation in the western Atlantic, a region associated with the southward flow of anthropogenic DIC in the deep western boundary current. The OCIM also has slightly larger anthropogenic CO_2-driven DIC accumulation rates in the intermediate and mode water formation regions of the subantarctic Southern Ocean and northwest Pacific than the GOBMs.

The climate-driven anthropogenic DIC accumulation can also be isolated in the GOBMs (Figure 7e). This component is seen to be quite small, with the primary feature being a very slight enhancement of anthropogenic DIC accumulation throughout much of the Southern Hemisphere, especially in the Pacific Ocean (Figure 7e; this feature is also seen over the period 1994–2007 in Figure S6 of the Supporting Information S1). These changes could be related to changes in the Southern Hemisphere mid-latitude westerly winds (Swart & Fyfe, 2012; Waugh et al., 2013) which control anthropogenic DIC uptake in the Southern Ocean by controlling the wind-driven Ekman transport and subduction of anthropogenic DIC in mode and intermediate waters, and the upwelling of anthropogenic DIC-free waters south of the polar front (Ito et al., 2010). No other RECCAP2 product yields a direct estimate of the climate-driven anthropogenic DIC accumulation for comparison to the GOBMs, but the eMLR-C* (Figure 7b) and OCIM (Figure 7d) estimates can be subtracted to yield a rough approximation of this component (Figure 7f). This quantity is identical to the so-called "anomalous change" in the anthropogenic carbon inventory derived by Gruber et al. (2019a, 2019b) for the eMLR-C* product. This estimate produces more coherent spatial patterns than the GOBMs, with DIC accumulation in the South Atlantic and most of the mid- to low-latitude oceans, along with DIC loss in the subpolar North Atlantic and Pacific and Indian sectors of the Southern Ocean (Figure 7f). While it is tempting to attribute these patterns to climate variability, the difference between the eMLR-C* and OCIM products is similar in magnitude to the biases of the eMLR-C* method identified from testing the method with synthetic data from a GOBM (Clement & Gruber, 2018). Combined with structural biases in the OCIM (such as neglect of seasonality and small-scale circulation features), means that the uncertainty of the values in Figure 7f is likely larger than their mean. Nevertheless, a recent update of the eMLR-C* estimates by Müller et al. (2023) also suggests substantial climate-driven variability in the oceanic storage of anthropogenic carbon similar to that shown in Figure 7f.

Regardless of their different spatial patterns, both the GOBMs (Figure 7e) and the eMLR-C*-OCIM difference (Figure 7f) suggest that the climate-driven anthropogenic DIC uptake is much smaller than the CO_2-driven anthropogenic DIC uptake. This is likely to hold true while atmospheric CO_2 concentrations continue to rise exponentially, but the influence of climate change may become more influential once atmospheric CO_2 concentrations plateau and start to decline (Ridge & McKinley, 2021).

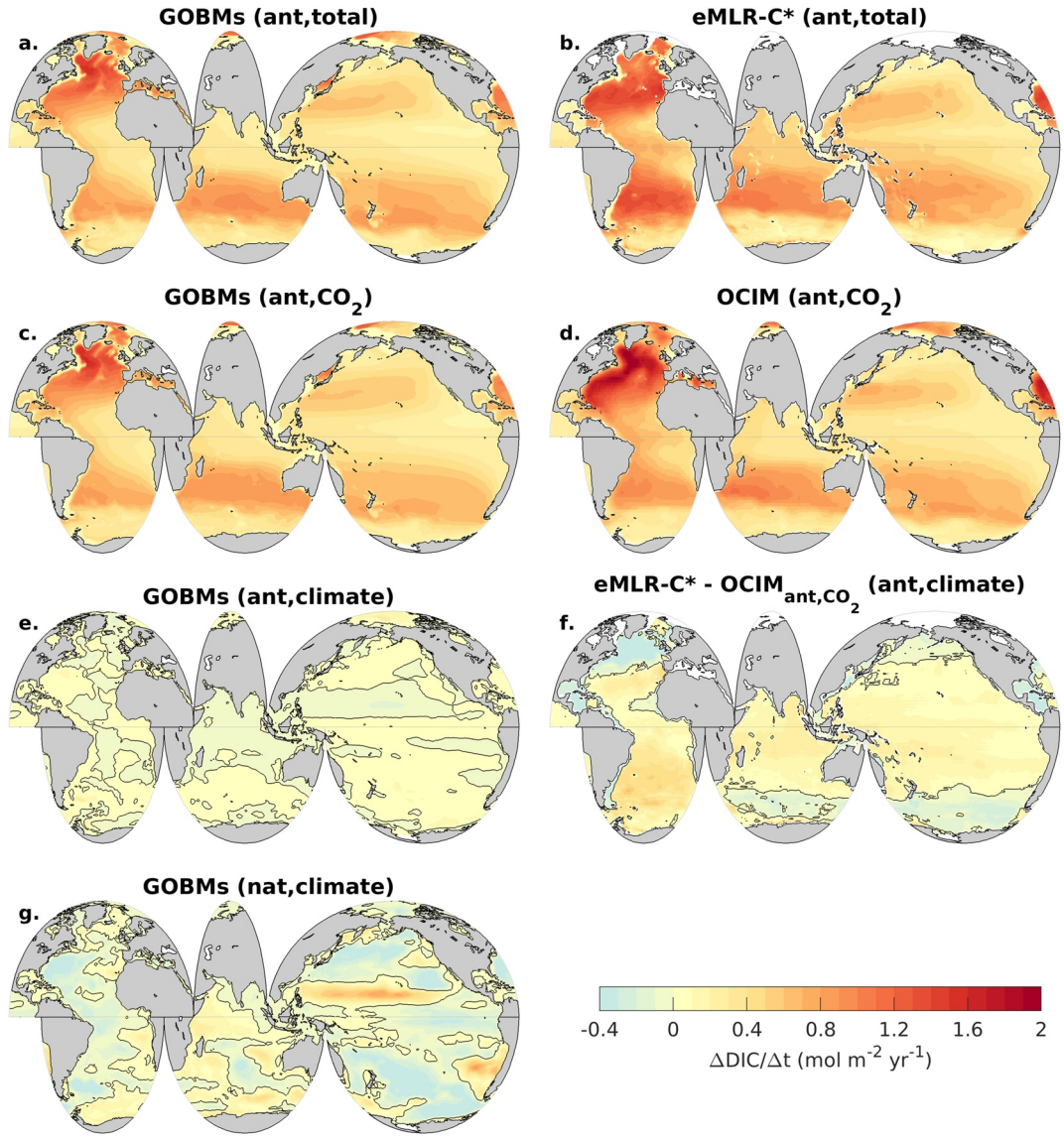

Figure 7. Vertically integrated rate of dissolved inorganic carbon (DIC) storage broken down into components using combinations of global ocean biogeochemical model (GOBM) simulations (left column) and from other models and products (right column). The top row is the rate of total anthropogenic DIC accumulation from (a) GOBMs (simulations A–D) and from (b) the eMLR-C* product. Note that the GOBMs cover the entire RECCAP2 period 1985–2018 while the eMLR-C* product covers only 1994–2007. The second row is the rate of anthropogenic CO_2-driven DIC accumulation from (c) the GOBMs (simulations C–B) and (d) the ocean circulation inverse model (OCIM) (simulations C–B). The third row shows the storage rate of the climate-driven anthropogenic DIC accumulation, determined from (e) the GOBMs using simulations (A–D)–(C–B), and from (f) the difference between the eMLR-C* product and the OCIM anthropogenic CO_2-driven component. The bottom row shows (g) the effect of climate-driven variability on natural DIC accumulation, from simulations D–B in the GOBMs. GOBM results are the average of all models that are available for that combination of simulations, except for the CCSM (see Table S1 in Supporting Information S1). The zero contour is shown as a solid line in all plots. Figure S6 in Supporting Information S1 shows a version of this figure over the period 1994–2007 for all products.

The GOBMs are the only RECCAP2 product which can directly diagnose the DIC accumulation due to the effects of climate variability on natural DIC cycling (Figure 7g). This component is substantially larger than the climate-driven anthropogenic DIC accumulation in the GOBMs, and shows more coherent spatial patterns, with reductions in natural DIC in the western boundary current regions of the North Atlantic and North Pacific during the RECCAP2 period. This explains in part why the GOBMs have smaller total DIC accumulation in these regions compared to the OCIM (cf., Figure 5). The GOBMs also lost substantial amounts of natural DIC

Table 2
Net Sea-Air CO_2 Flux and Its Components From RECCAP2 Products and the First RECCAP Analysis

$F_{sea\text{-}air}$	Globally integrated flux (Pg C yr^{-1})
GOBMs[a]	-1.9 ± 0.3
pCO_2 products (UOEX)	-1.5 ± 0.2 (-1.9 for UOEX)
OCIM	-2.3 ± 0.2
eMLR-C*[b]	-2.6 ± 0.3
RECCAP[c]	-1.6 ± 0.5
F_{ant} ($F_{ant,CO2} + F_{ant,\ climate}$)[d]	
GOBMs	-2.0 ± 0.2 (-2.0 ± 0.2–0.03 ± 0.03)
OCIM	-2.3 ± 0.1 (-2.3 ± 0.1 + ND)
eMLR-C*	-2.6 ± 0.3 (ND − 0.2[e])
RECCAP[c]	-2.0 ± 0.6
F_{nat} ($F_{land\text{-}sea,ss} + F_{nat,\ climate}$)[d]	
GOBMs	0.0 ± 0.2[f] (-0.11 ± 0.25[g] $+ 0.1 \pm 0.1$)
RECCAP[c]	ND (0.45 ± 0.2 + ND)

Note. Numbers are for the time period 1990–2009, except for the eMLR-C* product which is for 1994–2007. ND indicates no data for that particular product.

[a]GOBMs corrected for drift + bias by subtracting simulation B from simulation A. [b]Change in ocean interior anthropogenic DIC for the period 1994–2007. [c]From Wanninkhof et al. (2013). [d]Sum of components may not add up to total due to rounding errors and/or model drifts. [e]Difference between eMLR-C* F_{ant} and OCIM $F_{ant,CO2}$. [f]From Simulation D, also includes model drifts and biases. [g]$F_{land\text{-}sea}$ from GOBMs that resolve river and/or burial fluxes only.

in the South Pacific and the Pacific sector of the Southern Ocean over the RECCAP2 period. In contrast, climate variability drove an accumulation of DIC in the GOBMs in the eastern South Pacific near South America, and in a zonal strip of the western tropical North Pacific near 15°N.

In all, the results in Figure 7 indicate good agreement on the magnitudes and spatial patterns of anthropogenic DIC accumulation in the ocean from a variety of methods, and that the majority of anthropogenic DIC accumulation is from the atmospheric CO_2 increase, with small changes attributable to climate change and/or variability. The dominance of the anthropogenic component in DIC accumulation in the GOBMs stems from the dominance of the anthropogenic component of the air-sea CO_2 fluxes in these models (Figures 3 and 4). It should be noted, however, that this component is less dominant in the observation-based estimates. For example, in the pCO_2 products the climate-driven natural component of air-sea CO_2 fluxes is much more variable than in the GOBMs (Figure 4). The ECCO-Darwin model, which is tuned to interior DIC observations, also exhibits much more variability than the GOBMs, both in terms of the temporal variability of the air-sea CO_2 fluxes and in the spatial variability of DIC accumulation rates (Figures 2 and 5). However, the ECCO-Darwin results are subject to the caveats discussed above regarding the potential for assimilation-induced model drifts to affect their results.

4. Discussion

4.1. Comparison of the Global Ocean CO_2 Sink in RECCAP2 Versus RECCAP

Here, we assess differences between the results of RECCAP2 and the original RECCAP for the common period 1990–2009 covered by each analysis. Section 4.3 provides an updated "best estimate" of the ocean CO_2 sink for the period 2001–2018 from RECCAP2. Table S3 in Supporting Information S1 also provides an analysis of fluxes across different time periods, as well as a comparison to regional sea-air CO_2 fluxes.

For the nominal period 1990–2009, the globally integrated net sea-air CO_2 flux varies from -1.5 ± 0.2 to -2.6 ± 0.3 PgC yr^{-1} in different products considered for RECCAP2 (Table 2). This compares to the RECCAP estimate of -1.6 ± 0.5 PgC yr^{-1} for $F_{sea\text{-}air}$. Much of the differences in $F_{sea\text{-}air}$ among the RECCAP2 products is due to the fact that they resolve different components of the sea-air CO_2 flux. Table 2 presents these components separately in order to better assess the level of agreement or disagreement among the RECCAP2 products and the original RECCAP analysis.

Anthropogenic CO_2 fluxes from RECCAP2 products range from -2.0 ± 0.2 PgC yr^{-1} in the GOBMs to -2.6 ± 0.3 PgC yr^{-1} in the eMLR-C* product, with a middle value of -2.3 ± 0.1 PgC yr^{-1} in the OCIM. These estimates are larger, but not significantly so, than the original RECCAP study, which estimated an anthropogenic CO_2 flux of -2.0 ± 0.6 PgC yr^{-1} (W2013). The original RECCAP value was for the total anthropogenic CO_2 flux, and did not separately report values for the CO_2-driven and climate-driven anthropogenic CO_2 fluxes components. For RECCAP2, the GOBMs and OCIM estimate that the CO_2-driven anthropogenic flux ($F_{ant,CO2}$) is -2.0 ± 0.2 PgC yr^{-1} and -2.3 ± 0.1 PgC yr^{-1}, respectively. The climate-driven anthropogenic flux is negligible in the GOBMs at -0.03 ± 0.03 PgC yr^{-1}. If we interpret the difference between the eMLR-C* and the OCIM as representing $F_{ant,CO2}$ (e.g., Gruber et al., 2019a, 2019b), then $F_{ant,CO2}$ is slightly larger at 0.2 PgC yr^{-1} (Table 2), but this estimate likely carries >100% uncertainty.

Globally integrated natural sea-air CO_2 fluxes consist of the component that balances the net land-sea carbon flux at steady-state ($F_{land\text{-}sea,ss}$) and the climate-driven natural CO_2 flux ($F_{nat,\ climate}$). For RECCAP2, both of these components were assessed in the GOBMs. $F_{nat,\ climate}$ is small but positive in the GOBMs, at a value of 0.1 ± 0.1 PgC yr^{-1} over the 1990–2009 period (Table 2). The mechanisms responsible for this outgassing

of natural CO_2 have not been assessed here, but likely include a combination of ocean warming and circulation changes (DeVries, 2022; Le Quéré et al., 2010; Terhaar et al., 2022). RECCAP did not assess climate-driven fluxes of natural CO_2, so cannot provide a comparison to the RECCAP2 models. The RECCAP assessment did report an estimate of $F_{\text{land-sea,ss}}$ of 0.45 PgC yr^{-1}, which was adopted from a joint global ocean-atmosphere inversion model (Jacobson et al., 2007). Several of the RECCAP2 GOBMs do not include a representation of land-sea carbon fluxes, but those that do estimate a $F_{\text{land-sea,ss}}$ of -0.11 ± 0.25 PgC yr^{-1} (Table 2). This is far less than the RECCAP value and less than a recent global assessment of 0.65 ± 0.3 PgC yr^{-1} (Regnier et al., 2022), and is likely due to the incomplete representation of riverine and coastal carbon fluxes in GOBMs, which is a known shortcoming of these models (e.g., Hauck et al., 2020; Resplandy et al., 2023). Nonetheless, we report the $F_{\text{land-sea}}$ values from the GOBMs to illustrate that our ability to represent this flux in models is still in the developmental stage, and has not progressed much since the first RECCAP assessment.

4.2. Additional Uncertainties and Biases in Estimates of the Global Ocean CO_2 Sink

The uncertainties reported throughout this study are based on the spread of values in different product ensembles. This ensemble spread does not always capture the full uncertainty associated with each product or method, since ensemble members often share structural uncertainties due to common assumptions and biases. Before reporting our updated best estimate of the contemporary oceanic CO_2 sink in Section 4.3, we will briefly consider some of these additional uncertainties and attempt to estimate their magnitude for each class of products. We focus here on uncertainties that affect the multi-decadal average air-sea fluxes derived from these products, and not their interannual or decadal variability.

The pCO_2-observation products suffer from structural uncertainties and biases due to sparse data coverage, as well as their algorithms, parameterizations and input data. Data coverage for these products has significantly improved since roughly the year 2000, and these products appear to reliably reconstruct the mean and seasonal cycle of the open-ocean sea-air CO_2 fluxes at their relatively coarse spatial and temporal resolution (Gloege et al., 2021). However, limitations of these products are evident in the coastal regions where spatial and temporal variability of air-sea CO_2 fluxes is large (Sharp et al., 2022), as well as in the high latitudes such as the Southern Ocean where seasonal biases in sampling are most pronounced (Gray et al., 2018). Although some products have been developed to better resolve coastal air-sea CO_2 fluxes at appropriate resolution (e.g., Roobaert et al., 2019) and to integrate new data streams at high latitudes (Bushinsky et al., 2019), integrating these regions into global pCO_2 products is still in its beginning stages (Fay et al., 2021; Landschützer et al., 2020; Roobaert et al., 2023).

The parameterization of air-sea CO_2 fluxes in these products is another source of uncertainty and potential bias. Almost all of the pCO_2 products use a quadratic relationship between wind speed and gas transfer velocity, which is an empirical approximation of complex physics governing the interaction between winds, waves, currents, and gas transfer (e.g., McGillis et al., 2001; Shin et al., 2022). This relationship is not appropriate under all conditions, such as very low or very high wind speeds (Wanninkhof & McGillis, 1999; Wanninkhof et al., 2009). Moreover, the air-sea CO_2 flux calculations from pCO_2 products ignore small-scale temporal variability (e.g., diurnal and day-to-day variability) that could be an important contributor to CO_2 fluxes, especially given nonlinearities between the wind speed and gas transfer velocity (Bates & Merlivat, 2001; Djeutchouang et al., 2022; Sutton et al., 2021). Poor understanding of the impact of sea ice on air-sea CO_2 exchange contributes to large uncertainty in the polar oceans (Watts et al., 2022). Furthermore, differences between the temperature and salinity of the thin surface "skin" layer of the ocean and the bulk of the surface mixed layer could introduce significant biases into sea-air CO_2 flux calculations at global scales (Watson et al., 2020). None of these uncertainties and biases are captured by the ensemble uncertainty reported here. Studies suggest that these issues could lead to additional uncertainties on the order of 30% (Bushinsky et al., 2019; Landschützer et al., 2014; Roobaert et al., 2018; Wanninkhof, 2007; Watson et al., 2020; Woolf et al., 2019), or around ± 0.6 PgC yr^{-1} in the globally integrated net air-sea CO_2 flux.

GOBMs also suffer from structural biases. For one, GOBMs are seldom spun up to equilibrium under preindustrial atmospheric CO_2 concentrations, both because of computational constraints and because long spin-up times tend to accentuate errors in modeled circulation and biogeochemistry (Séférian et al., 2016). This may lead to biases in the ocean chemical buffering capacity and the rate of oceanic CO_2 uptake (Bronselaer et al., 2017; Terhaar et al., 2022, 2023). Even seemingly small inconsistencies in how the models are initialized and spun up can have relatively large impacts on air-sea CO_2 fluxes in these models (Séférian et al., 2016). GOBMs also

Table 3
"Best Estimate" of Ocean Carbon Sink Components Averaged Over the Time Period 2001–2018

Sea-air CO_2 flux component	Value (PgC yr^{-1})	Reported uncertainty	Additional uncertainty (estimated)	Source
$F_{sea\text{-}air}$	−1.9	±0.2	±0.6	pCO_2 products
$F_{ant,CO2}$	−2.7	±0.1	±0.3	OCIM
$F_{land\text{-}sea,ss}$	+0.65	±0.3	–	Regnier et al. (2022)
$F_{climate}$	+0.1	±0.1	±0.3	GOBMs

have known biases in their representation of physical processes such as ocean ventilation and overturning, due to their coarse resolution and parameterization of unresolved processes such as mixing and eddies (Doney et al., 2004; Gent, 2016; Large et al., 1994). As an example of the effects of such parameterizations, the rate of Atlantic Meridional Overturning Circulation (AMOC) in the RECCCAP2 GOBMs ranges from 3 to 24 Sv for models that all use similar surface forcing (Table S1 in Supporting Information S1), compared to an observed AMOC of roughly 17–18 Sv (Frajka-Williams, 2015). Another source of bias is that coarse-resolution GOBMs do not resolve coastal processes, nor do they fully resolve the processes and fluxes of carbon from terrestrial to marine environments, or at the sediment-water interface, which we have here called the net land-sea carbon fluxes. Despite these issues, GOBMs have great utility for understanding the processes that limit the rate of oceanic anthropogenic CO_2 uptake (e.g., Sarmiento et al., 1992), and they remain one of the few tools for understanding how climate change is influencing air-sea CO_2 fluxes, since they can be run both with and without climate variability, as done here and in previous studies (e.g., DeVries et al., 2019; Le Quéré et al., 2010).

Data assimilation is a promising approach for constraining the global ocean carbon sink and its variability, but the assimilation models used here come with caveats and biases that can limit their utility. The OCIM does not resolve biological carbon cycling, nor does it resolve climate-driven variability in ocean circulation and biogeochemistry. For these reasons its usefulness is primarily in constraining the CO_2-driven anthropogenic DIC uptake by the ocean, $F_{ant,CO2}$. However, the coarse spatial resolution and lack of seasonal variability and biological carbon cycling in the OCIM could still bias its estimates of $F_{ant,CO2}$. Seasonality is known to influence rates of anthropogenic CO_2 uptake (Rodgers et al., 2008), and this variability will become more important as the ocean acidifies and the Revelle buffer factor increases, enhancing the biologically and temperature-driven seasonal variations in seawater chemistry (Fassbender et al., 2018, 2022; Hauck & Völker, 2015; Rodgers et al., 2023). The influence of missing seasonality, small-scale circulation features, and biology on anthropogenic CO_2 uptake by the OCIM has not been quantified, but here we adopt an ad hoc estimate of about 10%–15%, or an additional 0.3 PgC yr^{-1} uncertainty to the OCIM estimates of $F_{ant,CO2}$.

The ECCO-Darwin assimilation model improves on the OCIM in some respects by running at a higher spatial resolution (Table S1 in Supporting Information S1), including biological carbon cycling and ecology of lower trophic levels, and resolving seasonal to interannual variability. However, it too suffers from some serious biases. For one, the model is not fully spun up to equilibrium under preindustrial conditions before assimilation. The biogeochemical assimilation period itself is short (starting in 1992) and therefore introduces drifts into the model as the biogeochemical parameters adjust from their initial values. Furthermore, the model has an unrealistically large sedimentary carbon burial flux (1.3 PgC yr^{-1}) which is not balanced by river carbon inputs. This alone could bias the ECCO-Darwin sea-air CO_2 fluxes by over 1 PgC yr^{-1}.

The eMLR-C* product provides an estimate of the oceanic anthropogenic CO_2 sink that is unique from the other RECCAP2 products in using interior DIC observations (Clement & Gruber, 2018). However, significant uncertainties remain with this method as with others. Validation of the approach using output from a biogeochemical model demonstrated that the eMLR-C* approach accurately reconstructed the anthropogenic DIC inventory change within about 10% at a global scale (Clement & Gruber, 2018). Using actual ocean DIC observations that are considerably noisier than model output, Gruber et al. (2019a, 2019b) estimated an uncertainty of ±0.3 PgC yr^{-1}. Unaccounted-for uncertainties that could raise this estimate include the unassessed influence of anthropogenic perturbations to the land-sea carbon fluxes (e.g., Regnier et al., 2013), and the growing influence of seasonal variability in affecting anthropogenic carbon uptake at high CO_2 concentrations (e.g., Hauck & Völker, 2015).

4.3. A Best Estimate of the Ocean CO_2 Sink From 2001 to 2018

As was done for the original RECCAP, we offer here a "best estimate" of the oceanic CO_2 sink and its components in the contemporary ocean (Table 3). We focus on the period 2001–2018, when there is improved data coverage and forcing fields for pCO_2 products and GOBMs, and to update our estimates from the original RECCAP period of 1990–2009. For the net sea-air CO_2 flux, $F_{sea\text{-}air}$, we adopt the estimate from the pCO_2-observation products of −1.9 PgC yr^{-1}. The uncertainty on this flux derived from the pCO_2-product ensemble is ±0.2 PgC yr^{-1}, but this small uncertainty likely derives from the similarities in data processing and input data used for sea-air CO_2

flux algorithms that are common to all products (Table S2 in Supporting Information S1). As discussed above (Section 4.2) we estimate an additional ±0.6 PgC yr^{-1} uncertainty on this flux to account for factors such as the wind speed dependency of the gas transfer velocity, the unresolved influences of small-scale variability, and sampling limitations in coastal and high-latitude regions.

For the anthropogenic CO_2-driven component of the sea-air CO_2 flux, $F_{ant,CO2}$, we use the estimate from the OCIM of −2.7 PgC yr^{-1}. We use the OCIM, rather than the GOBMs for this component as the OCIM is a data-assimilated model that accurately represents ocean ventilation and overturning circulation, which is the leading order process for oceanic anthropogenic CO_2 uptake (Davila et al., 2022; Iudicone et al., 2016; Orr et al., 2001; Sarmiento et al., 1992; Terhaar et al., 2021). Also, the OCIM is fully spun up to chemical equilibrium under preindustrial conditions unlike the GOBMs. The OCIM estimate comes with a small ensemble uncertainty of ±0.1 PgC yr^{-1} from two different configurations of the OCIM. As discussed above (Section 4.2) we adopt an ad hoc value of ±0.3 PgC yr^{-1} for additional uncertainties from the influence of unresolved processes such as small-scale circulation features, seasonal variability, and biological processes.

The preindustrial net land-sea carbon fluxes lead to a net outgassing of CO_2 at steady, $F_{land\text{-}sea,ss}$. Despite the large magnitude of this flux it is not well represented in any of the RECCAP2 products, so here we adopt the recent bottom-up estimate of 0.65 PgC yr^{-1} from Regnier et al. (2022). This is larger than the RECCAP estimate of 0.45 PgC yr^{-1} (W2013), but also comes with a substantial uncertainty of ±0.3 PgC yr^{-1}. This uncertainty is estimated by propagating errors in different estimates of the carbon fluxes along the land-ocean-aquatic continuum (Regnier et al., 2022), and is likely a lower-bound uncertainty estimate although we do not attempt to estimate additional unresolved uncertainties here.

Finally, the smallest and relatively most uncertain component of the contemporary global sea-air CO_2 flux is that driven by climate variability and change, $F_{climate}$. The GOBMs provide the only direct estimate of this component, averaging 0.1 PgC yr^{-1}. The ensemble uncertainty of this flux is ±0.1 PgC yr^{-1}, but this is an underestimate of the true uncertainty as it derives only from the GOBM ensemble standard deviation. How much additional uncertainty there is can be roughly estimated by comparing the climate-driven trend in the GOBMs with that derived by subtracting modeled anthropogenic trends from the pCO_2 products (see Section 3.1.2). The pCO_2 products suggest a climate-driven trend of nearly −0.3 PgC yr^{-1} $decade^{-1}$ from 2001 to 2018, compared to climate-driven trend near 0 in the GOBMs (cf., Figure 4). We thus estimate an additional uncertainty of ±0.3 PgC yr^{-1} on $F_{climate}$, due to the influence of climate variability and change on the global ocean carbon sink that may not be fully resolved by the GOBMs. This is only an estimate, and must be caveated by the fact that the trends in the pCO_2 products that are here attributed to climate variability may also be inaccurate (e.g., Gloege et al., 2021; Hauck et al., 2023).

5. Conclusions

The RECCAP2 analysis has provided a comprehensive view of the global ocean CO_2 sink for the period 1985–2018 from a variety of model and observation-based products. Here, we summarize the main findings of the RECCAP2 global ocean analysis and provide recommendations for future work to target the most critical uncertainties in the global ocean carbon sink.

To summarize our findings for the mean, variability, and trends of the ocean CO_2 sink over the RECCAP2 period:

- *Mean*: The mean ocean net sea-air CO_2 flux from 1985 to 2018 is −1.6 ± 0.2 PgC yr^{-1} as diagnosed by pCO_2-observation based air-sea CO_2 flux products. The dominant component of this flux is the oceanic uptake of anthropogenic CO_2, which is estimated at −2.1 ± 0.3 PgC yr^{-1} by the ensemble of GOBMs, and −2.4 ± 0.1 PgC yr^{-1} by the data-assimilated OCIM. The second largest component of the global air-sea CO_2 flux is the outgassing of terrestrially derived CO_2, which is estimated at 0.65 ± 0.3 PgC yr^{-1} (Regnier et al., 2022) but is not yet fully resolved by RECCAP2 models.
- *Trends*: The trend in the global air-sea CO_2 flux from 1985 to 2018 ranges from −0.26 ± 0.04 PgC yr^{-1} $decade^{-1}$ in the GOBMs to −0.38 ± 0.24 PgC yr^{-1} $decade^{-1}$ in the pCO_2 products. Over the 2001–2018 period, when the pCO_2-based estimates benefit from improved data coverage, they predict a strengthening trend in the ocean carbon sink of −0.61 ± 0.12 PgC yr^{-1} $decade^{-1}$. This is driven primarily by the trend in anthropogenic carbon uptake of −0.41 ± 0.03 PgC yr^{-1} $decade^{-1}$ as diagnosed by the OCIM. The remaining trend is inferred to be climate-forced. This putative climate-forced strengthening of the ocean carbon sink since 2001 in the

pCO_2 products is not apparent in the GOBMs, and thus the robustness of and the reasons for this trend remain unclear.

- *Variability*: In the GOBM simulations, the interannual to decadal variability of the global carbon sink is mainly driven by climate variability, with the climate-driven variability exceeding the CO_2-forced variability by 2–3 times. GOBMs suggest that the climate-driven variability is about 4%–8% of the global mean carbon sink, but the pCO_2 products exhibit larger variability that is about 9%–14% of the global mean flux.

It should be clear from this analysis that while we have in some respects a good understanding and quantification of the global ocean CO_2 sink, there are other areas that are considerably less well understood. We suggest that research in the next several years should focus on four critical areas:

1. The land-sea carbon flux, which represents the difference between the influx of terrestrial carbon to the ocean and the burial of carbon in marine sediments, is the second largest component of the global air-sea CO_2 flux, but is poorly represented in most models and is less well studied than the anthropogenic CO_2 fluxes. There is a critical need to increase both direct and indirect observations of these fluxes, and to better integrate these fluxes into carbon cycle models, so that more constraints can be brought to bear on the magnitude of the land-sea carbon fluxes. For GOBMs, this will require better coupling between the terrestrial and oceanic environments, and better representation of processes at the land-sea interface, such as terrestrial carbon burial and transformation to CO_2 on continental shelves and in estuaries (Regnier et al., 2022). The pCO_2 products need to represent unique dynamics of the sea-air CO_2 fluxes in different coastal regions, including their high spatial and temporal variability (e.g., Sharp et al., 2022), and to merge these fluxes with the open-ocean products in a consistent way. A lack of observations in some coastal regions, particularly in the tropical oceans (Roobaert et al., 2023), could hinder these efforts and should be a target for new observational programs.
2. The climate-driven sea-air CO_2 fluxes remain highly uncertain and inconsistently captured across different products, making it difficult to ascertain the effect that climate change is having on the ocean carbon sink. The pCO_2-based products require further validation to assess if their algorithms are introducing biases that can be incorrectly attributed to climate variability (e.g., Denvil-Sommer et al., 2021; Gloege et al., 2021; Hauck et al., 2023), and if so, further refinement of these algorithms is needed. GOBMs require higher resolution to ensure that they are correctly capturing all the relevant scales of climate-driven variability. Given the need to also lengthen the spinup phase of these models to reach preindustrial equilibrium, achieving a higher resolution may require substantial technological or methodological innovations.
3. Data assimilation models provide a potential avenue for alleviating some of the structural errors and biases in ocean biogeochemical models (e.g., Fennel et al., 2022). They also have the ability to integrate multiple data sources, which together can provide stronger constraints on global carbon cycling than those derived from a single data source such as the purely pCO_2-based or DIC-based products. Future assimilation systems should harness the complementary strengths of the assimilation models used here. Such a system needs to represent the multi-scale variability of physical and biological processes like the ECCO-Darwin, while maintaining the ability of the OCIM to accurately capture the oceanic mean state by incorporating information from multiple circulation tracers and performing long-timescale (∼1,000 years) assimilations. Incorporating new information into these models from sources such as atmospheric oxygen (e.g., Manning & Keeling, 2006; Resplandy et al., 2019) and stable carbon isotopes (Quay et al., 1992) could help further constrain sea-air CO_2 fluxes and their anthropogenic- and climate-driven components.
4. Perhaps most critically, it is imperative to maintain and expand the ocean observing systems that form the backbone of our assessments of the ocean carbon sink, including maintaining the network of surface ocean pCO_2 measurements through programs such as SOCONET (Wanninkhof et al., 2019), and data assembly and quality control programs such as SOCAT (Bakker et al., 2016). It is also critical to maintain regular sampling of ocean carbonate system parameters and transient tracers by repeat hydrography programs such as GO-SHIP (Talley et al., 2016). Finally, it is important to support emerging technologies, including autonomous platforms such as biogeochemical Argo (Claustre et al., 2020) and uncrewed surface vehicles (Sutton et al., 2021), that can fill observational gaps in hostile and remote environments.

Conflict of Interest

The authors declare no conflicts of interest relevant to this study.

Acknowledgments
TD acknowledges support from the US National Science Foundation through Grant OCE-1948955. RW and BR are supported by funding from NOAA's Global Ocean Monitoring and Observations (GOMO) Program. The CICOES and PMEL contributions to this work are numbers 2023-1260 and 5497, respectively. JDM, LG, and NG acknowledge support from the European Union's Horizon 2020 research and innovation programme under Grant agreement no. 821003 (project 4C) and no. 820989 (project COMFORT). JH acknowledges funding from the Initiative and Networking Fund of the Helmholtz Association (Helmholtz Young Investigator Group Marine Carbon and Ecosystem Feedbacks in the Earth System (MarESys), Grant VH-NG-1301) and from ERC-2022-STG OceanPeak, Grant agreement 101077209. DC acknowledges support from the NASA Carbon Cycle and Ecosystems (CCE) program under Grant 80NSSC22K0154. SCD acknowledges support from the NSF Center for Chemical Currencies of a Microbial Planet (C-CoMP) (NSF Award 2019589). SAH was supported by a European Research Council Consolidator Grant (GOCART, agreement number 724416). PL was supported by Research Foundation Flanders (FWO) contract I001821N. CN acknowledges funding from the European Union's Horizon 2020 research and innovation programme under Grant agreement No 820989 (project COMFORT). LP acknowledges funding from the project PA 3075/2-1 by the German Research Foundation and the North German Supercomputing Alliance (HLRN) for providing computing power for the experiments. FFP was supported by the BOCATS2 project (PID2019-104279GB-C21) funded by MCIN/AEI/10.13039/501100011033. KBR was supported by the Institute for Basic Sciences (IBS), Republic of Korea, under IBS-R028-D1. JS acknowledges funding from the Research Council of Norway (Grant 270061) and computational/storage resources provided by UNINET/sigma2 (nn/ns2980k). JTH was funded by the Woods Hole Oceanographic Institution Postdoctoral Scholar Program, the European Union's Horizon 2020 research and innovation program under grant agreement 821003 (project 4C, Climate-Carbon Interactions in the Current Century), and the Swiss National Science Foundation under Grant 200020_200511. CLQ acknowledges funding from the European Union project 4C (Grant 821003) and the Royal Society (Grant RP\R1\191063), and support from UEA's High Performance Computing services. TTTC and MG acknowledge financial support by the European Copernicus Marine Environment Monitoring Service (CMEMS) MOB-TAC project for the joint development with F. Chevallier of the CMEMS-LSCE-FFNN model.

Data Availability Statement

The RECCAP2 ocean data collection can be found in Müller (2023).

References

Andrews, O. D., Bindoff, N. L., Halloran, P. R., Ilyina, T., & Le Quéré, C. (2013). Detecting an external influence on recent changes in oceanic oxygen using an optimal fingerprinting method. *Biogeosciences*, *10*(3), 1799–1813. https://doi.org/10.5194/bg-10-1799-2013

Archer, D. (2005). Fate of fossil fuel CO_2 in geologic time. *Journal of Geophysical Research*, *110*(C9), C09S05. https://doi.org/10.1029/2004jc002625

Bacastow, R. B. (1976). Modulation of atmospheric carbon dioxide by the Southern Oscillation. *Nature*, *261*(5556), 116–118. https://doi.org/10.1038/261116a0

Bakker, D. C., Pfeil, B., Landa, C. S., Metzl, N., O'brien, K. M., Olsen, A., et al. (2016). A multi-decade record of high-quality fCO_2 data in version 3 of the surface ocean CO_2 Atlas (SOCAT). *Earth System Science Data*, *8*(2), 383–413.

Bates, N. R., & Merlivat, L. (2001). The influence of short-term wind variability on air-sea CO_2 exchange. *Geophysical Research Letters*, *28*(17), 3281–3284. https://doi.org/10.1029/2001gl012897

Bennington, V., Gloege, L., & McKinley, G. A. (2022). Variability in the global ocean carbon sink from 1959 to 2020 by correcting models with observations. *Geophysical Research Letters*, *49*(14), e2022GL098632. https://doi.org/10.1029/2022gl098632

Bernardello, R., Marinov, I., Palter, J. B., Galbraith, E. D., & Sarmiento, J. L. (2014). Impact of Weddell Sea deep convection on natural and anthropogenic carbon in a climate model. *Geophysical Research Letters*, *41*(20), 7262–7269. https://doi.org/10.1002/2014gl061313

Bolin, B., & Eriksson, E. (1959). Changes in the carbon dioxide content of the atmosphere and sea due to fossil fuel combustion. *The Atmosphere and the Sea in Motion*, *1*, 30–142.

Brewer, P. G. (1978). Direct observation of the oceanic CO_2 increase. *Geophysical Research Letters*, *5*(12), 997–1000. https://doi.org/10.1029/gl005i012p00997

Broecker, W. S., Takahashi, T., Simpson, H. J., & Peng, T.-H. (1979). Fate of fossil fuel carbon dioxide and the global carbon budget. *Science*, *206*(4417), 409–418. https://doi.org/10.1126/science.206.4417.409

Bronselaer, B., Winton, M., Russell, J., Sabine, C. L., & Khatiwala, S. (2017). Agreement of CMIP5 simulated and observed ocean anthropogenic CO_2 uptake. *Geophysical Research Letters*, *44*(24), 212–298. https://doi.org/10.1002/2017gl074435

Burdige, D. J. (2007). Preservation of organic matter in marine sediments: Controls, mechanisms, and an imbalance in sediment organic carbon budgets? *Chemical Reviews*, *107*(2), 467–485. https://doi.org/10.1021/cr050347q

Bushinsky, S. M., Landschützer, P., Rödenbeck, C., Gray, A. R., Baker, D., Mazloff, M. R., et al. (2019). Reassessing Southern Ocean air-sea CO_2 flux estimates with the addition of biogeochemical float observations. *Global Biogeochemical Cycles*, *33*(11), 1370–1388. https://doi.org/10.1029/2019gb006176

Caldeira, K., & Duffy, P. B. (2000). The role of the Southern Ocean in uptake and storage of anthropogenic carbon dioxide. *Science*, *287*(5453), 620–622. https://doi.org/10.1126/science.287.5453.620

Canadell, J. G., Ciais, P., Gurney, K., Le Quéré, C., Piao, S., Raupach, M. R., & Sabine, C. L. (2011). An international effort to quantify regional carbon fluxes. *Eos, Transactions American Geophysical Union*, *92*(10), 81–82. https://doi.org/10.1029/2011eo100001

Canadell, J. G., Monteiro, P. M., Costa, M. H., Da Cunha, L. C., Cox, P. M., Alexey, V., et al. (2021). Global carbon and other biogeochemical cycles and feedbacks.

Carroll, D., Menemenlis, D., Adkins, J. F., Bowman, K. W., Brix, H., Dutkiewicz, S., et al. (2020). The ECCO-darwin data-assimilative global ocean biogeochemistry model: Estimates of seasonal to multidecadal surface ocean pCO_2 and air-sea CO_2 flux. *Journal of Advances in Modeling Earth Systems*, *12*(10), e2019MS001888. https://doi.org/10.1029/2019ms001888

Carroll, D., Menemenlis, D., Dutkiewicz, S., Lauderdale, J. M., Adkins, J. F., Bowman, K. W., et al. (2022). Attribution of space-time variability in global-ocean dissolved inorganic carbon. *Global Biogeochemical Cycles*, *36*(3), e2021GB007162. https://doi.org/10.1029/2021gb007162

Chau, T. T. T., Gehlen, M., & Chevallier, F. (2022). A seamless ensemble-based reconstruction of surface ocean pCO_2 and air–sea CO_2 fluxes over the global coastal and open oceans. *Biogeosciences*, *19*(4), 1087–1109. https://doi.org/10.5194/bg-19-1087-2022

Chen, C. T. A. (1982). On the distribution of anthropogenic CO_2 in the Atlantic and Southern oceans. *Deep-Sea Research, Part A: Oceanographic Research Papers*, *29*(5), 563–580. https://doi.org/10.1016/0198-0149(82)90076-0

Claustre, H., Johnson, K. S., & Takeshita, Y. (2020). Observing the global ocean with biogeochemical-Argo. *Annual Review of Marine Science*, *12*(1), 23–48. https://doi.org/10.1146/annurev-marine-010419-010956

Clement, D., & Gruber, N. (2018). The eMLR (C*) method to determine decadal changes in the global ocean storage of anthropogenic CO_2. *Global Biogeochemical Cycles*, *32*(4), 654–679. https://doi.org/10.1002/2017gb005819

Cole, J. J., Prairie, Y. T., Caraco, N. F., McDowell, W. H., Tranvik, L. J., Striegl, R. G., et al. (2007). Plumbing the global carbon cycle: Integrating inland waters into the terrestrial carbon budget. *Ecosystems*, *10*(1), 172–185. https://doi.org/10.1007/s10021-006-9013-8

Crisp, D., Dolman, H., Tanhua, T., McKinley, G. A., Hauck, J., Bastos, A., et al. (2022). How well do we understand the land-ocean-atmosphere carbon cycle? *Reviews of Geophysics*, *60*(2), e2021RG000736. https://doi.org/10.1029/2021rg000736

Davila, X., Gebbie, G., Brakstad, A., Lauvset, S. K., McDonagh, E. L., Schwinger, J., & Olsen, A. (2022). How is the ocean anthropogenic carbon reservoir filled? *Global Biogeochemical Cycles*, *36*(5), e2021GB007055. https://doi.org/10.1029/2021gb007055

Denvil-Sommer, A., Gehlen, M., & Vrac, M. (2021). Observation system simulation experiments in the Atlantic Ocean for enhanced surface ocean pCO_2 reconstructions. *Ocean Science*, *17*(4), 1011–1030. https://doi.org/10.5194/os-17-1011-2021

Denvil-Sommer, A., Gehlen, M., Vrac, M., & Mejia, C. (2019). LSCE-FFNN-v1: A two-step neural network model for the reconstruction of surface ocean pCO_2 over the global ocean. *Geoscientific Model Development*, *12*(5), 2091–2105. https://doi.org/10.5194/gmd-12-2091-2019

DeVries, T. (2014). The oceanic anthropogenic CO_2 sink: Storage, air-sea fluxes, and transports over the industrial era. *Global Biogeochemical Cycles*, *28*(7), 631–647. https://doi.org/10.1002/2013gb004739

DeVries, T. (2022b). The ocean carbon cycle. *Annual Review of Environment and Resources*, *47*(1), 317–341. https://doi.org/10.1146/annurev-environ-120920-111307

DeVries, T. (2022). Atmospheric CO_2 and sea surface temperature variability cannot explain recent decadal variability of the ocean CO_2 sink. *Geophysical Research Letters*, *49*(7), e2021GL096018. https://doi.org/10.1029/2021gl096018

DeVries, T., Holzer, M., & Primeau, F. (2017). Recent increase in oceanic carbon uptake driven by weaker upper-ocean overturning. *Nature*, *542*(7640), 215–218. https://doi.org/10.1038/nature21068

DeVries, T., Le Quéré, C., Andrews, O., Berthet, S., Hauck, J., Ilyina, T., et al. (2019). Decadal trends in the ocean carbon sink. *Proceedings of the National Academy of Sciences of the United States of America*, *116*(24), 11646–11651. https://doi.org/10.1073/pnas.1900371116

Djeutchouang, L. M., Chang, N., Gregor, L., Vichi, M., & Monteiro, P. (2022). The sensitivity of pCO_2 reconstructions to sampling scales across a Southern Ocean sub-domain: A semi-idealized ocean sampling simulation approach. *Biogeosciences*, *19*(17), 4171–4195. https://doi.org/10.5194/bg-19-4171-2022

Doney, S. C., Lindsay, K., Caldeira, K., Campin, J. M., Drange, H., Dutay, J. C., et al. (2004). Evaluating global ocean carbon models: The importance of realistic physics. *Global Biogeochemical Cycles*, *18*(3). https://doi.org/10.1029/2003gb002150

Drake, T. W., Tank, S. E., Zhulidov, A. V., Holmes, R. M., Gurtovaya, T., & Spencer, R. G. (2018). Increasing alkalinity export from large Russian Arctic rivers. *Environmental Science & Technology*, *52*(15), 8302–8308. https://doi.org/10.1021/acs.est.8b01051

Dunne, J. P., Sarmiento, J. L., & Gnanadesikan, A. (2007). A synthesis of global particle export from the surface ocean and cycling through the ocean interior and on the seafloor. *Global Biogeochemical Cycles*, *21*(4). https://doi.org/10.1029/2006gb002907

Dutkiewicz, S., Hickman, A. E., Jahn, O., Gregg, W. W., Mouw, C. B., & Follows, M. J. (2015). Capturing optically important constituents and properties in a marine biogeochemical and ecosystem model. *Biogeosciences*, *12*(14), 4447–4481. https://doi.org/10.5194/bg-12-4447-2015

Fassbender, A. J., Rodgers, K. B., Palevsky, H. I., & Sabine, C. L. (2018). Seasonal asymmetry in the evolution of surface ocean pCO_2 and pH thermodynamic drivers and the influence on sea-air CO_2 flux. *Global Biogeochemical Cycles*, *32*(10), 1476–1497. https://doi.org/10.1029/2017gb005855

Fassbender, A. J., Schlunegger, S., Rodgers, K. B., & Dunne, J. P. (2022). Quantifying the role of seasonality in the marine carbon cycle feedback: An ESM2M case study. *Global Biogeochemical Cycles*, *36*(6), e2021GB007018. https://doi.org/10.1029/2021gb007018

Fay, A. R., Gregor, L., Landschützer, P., McKinley, G. A., Gruber, N., Gehlen, M., et al. (2021). SeaFlux: Harmonization of air–sea CO_2 fluxes from surface pCO_2 data products using a standardized approach. *Earth System Science Data*, *13*(10), 4693–4710. https://doi.org/10.5194/essd-13-4693-2021

Feely, R. A., Takahashi, T., Wanninkhof, R., McPhaden, M. J., Cosca, C. E., Sutherland, S. C., & Carr, M. E. (2006). Decadal variability of the air-sea CO_2 fluxes in the equatorial Pacific Ocean. *Journal of Geophysical Research*, *111*(C8), C08S90. https://doi.org/10.1029/2005jc003129

Feely, R. A., Wanninkhof, R., Takahashi, T., & Tans, P. (1999). Influence of El Niño on the equatorial Pacific contribution to atmospheric CO_2 accumulation. *Nature*, *398*(6728), 597–601. https://doi.org/10.1038/19273

Fennel, K., Mattern, J. P., Doney, S. C., Bopp, L., Moore, A. M., Wang, B., & Yu, L. (2022). Ocean biogeochemical modelling. *Nature Reviews Methods Primers*, *2*(1), 76. https://doi.org/10.1038/s43586-022-00154-2

Forget, G. A. E. L., Campin, J. M., Heimbach, P., Hill, C. N., Ponte, R. M., & Wunsch, C. (2015). ECCO version 4: An integrated framework for non-linear inverse modeling and global ocean state estimation. *Geoscientific Model Development*, *8*(10), 3071–3104. https://doi.org/10.5194/gmd-8-3071-2015

Forster, P., Storelvmo, T., Armour, K., Collins, W., Dufresne, J.-L., Frame, D., et al. (2021). The Earth's energy budget, climate feedbacks, and climate sensitivity. In V. Masson-Delmotte, P. Zhai, A. Pirani, S. L. Connors, C. Péan, S. Berger, et al. (Eds.), *Climate change 2021: The physical science basis. Contribution of working group I to the sixth assessment report of the intergovernmental panel on climate change* (pp. 923–1054). Cambridge University Press. https://doi.org/10.1017/9781009157896.009

Frajka-Williams, E. (2015). Estimating the Atlantic overturning at 26 N using satellite altimetry and cable measurements. *Geophysical Research Letters*, *42*(9), 3458–3464. https://doi.org/10.1002/2015gl063220

Friedlingstein, P., Jones, M. W., O'Sullivan, M., Andrew, R. M., Bakker, D. C. E., Hauck, J., et al. (2022). Global carbon budget 2021. *Earth System Science Data*, *14*(4), 1917–2005. https://doi.org/10.5194/essd-14-1917-2022

Gent, P. R. (2016). Effects of Southern Hemisphere wind changes on the meridional overturning circulation in ocean models. *Annual Review of Marine Science*, *8*(1), 79–94. https://doi.org/10.1146/annurev-marine-122414-033929

Gloege, L., McKinley, G. A., Landschützer, P., Fay, A. R., Frölicher, T. L., Fyfe, J. C., et al. (2021). Quantifying errors in observationally based estimates of ocean carbon sink variability. *Global Biogeochemical Cycles*, *35*(4), e2020GB006788. https://doi.org/10.1029/2020gb006788

Gloege, L., Yan, M., Zheng, T., & McKinley, G. A. (2022). Improved quantification of ocean carbon uptake by using machine learning to merge global models and pCO_2 data. *Journal of Advances in Modeling Earth Systems*, *14*(2), e2021MS002620. https://doi.org/10.1029/2021ms002620

Gray, A. R., Johnson, K. S., Bushinsky, S. M., Riser, S. C., Russell, J. L., Talley, L. D., et al. (2018). Autonomous biogeochemical floats detect significant carbon dioxide outgassing in the high-latitude Southern Ocean. *Geophysical Research Letters*, *45*(17), 9049–9057. https://doi.org/10.1029/2018gl078013

Gregor, L., Lebehot, A. D., Kok, S., & Scheel Monteiro, P. M. (2019). A comparative assessment of the uncertainties of global surface ocean CO_2 estimates using a machine-learning ensemble (CSIR-ML6 version 2019a)–have we hit the wall? *Geoscientific Model Development*, *12*(12), 5113–5136. https://doi.org/10.5194/gmd-12-5113-2019

Gruber, N., Bakker, D. C., DeVries, T., Gregor, L., Hauck, J., Landschützer, P., et al. (2023). Trends and variability in the ocean carbon sink. *Nature Reviews Earth & Environment*, *4*(2), 119–134. https://doi.org/10.1038/s43017-022-00381-x

Gruber, N., Clement, D., Carter, B. R., Feely, R. A., Van Heuven, S., Hoppema, M., et al. (2019a). The oceanic sink for anthropogenic CO_2 from 1994 to 2007. *Science*, *363*(6432), 1193–1199. https://doi.org/10.1126/science.aau5153

Gruber, N., Landschützer, P., & Lovenduski, N. S. (2019b). The variable Southern Ocean carbon sink. *Annual Review of Marine Science*, *11*(1), 159–186. https://doi.org/10.1146/annurev-marine-121916-063407

Gruber, N., Sarmiento, J. L., & Stocker, T. F. (1996). An improved method for detecting anthropogenic CO_2 in the oceans. *Global Biogeochemical Cycles*, *10*(4), 809–837. https://doi.org/10.1029/96gb01608

Hall, T. M., Haine, T. W., & Waugh, D. W. (2002). Inferring the concentration of anthropogenic carbon in the ocean from tracers. *Global Biogeochemical Cycles*, *16*(4), 78-1–78-15. https://doi.org/10.1029/2001gb001835

Hauck, J., Nissen, C., Landschützer, P., Rödenbeck, C., Bushinsky, S., & Olsen, A. (2023). Sparse observations induce large biases in estimates of the global ocean CO_2 sink: An ocean model subsampling experiment. *Philosophical Transactions of the Royal Society A*, *381*(2249), 20220063. https://doi.org/10.1098/rsta.2022.0063

Hauck, J., & Völker, C. (2015). Rising atmospheric CO_2 leads to large impact of biology on Southern Ocean CO_2 uptake via changes of the Revelle factor. *Geophysical Research Letters*, *42*(5), 1459–1464. https://doi.org/10.1002/2015gl063070

Hauck, J., Zeising, M., Le Quéré, C., Gruber, N., Bakker, D. C. E., Bopp, L., et al. (2020). Consistency and challenges in the ocean carbon sink estimate for the global carbon budget. *Frontiers in Marine Science*, *7*, 1–22. https://doi.org/10.3389/fmars.2020.571720

Holzer, M., DeVries, T., & de Lavergne, C. (2021). Diffusion controls the ventilation of a Pacific Shadow Zone above abyssal overturning. *Nature Communications*, *12*(1), 1–13.

Iida, Y., Kojima, A., Takatani, Y., & Ishii, M. (2021). Global trends of ocean CO_2 sink and ocean acidification: An observation-based reconstruction of surface ocean inorganic carbon variables. *Journal of Oceanography*, *77*(2), 323–358. https://doi.org/10.1007/s10872-020-00571-5

Ishii, M., Feely, R. A., Rodgers, K. B., Park, G. H., Wanninkhof, R., Sasano, D., et al. (2014). Air–sea CO_2 flux in the Pacific Ocean for the period 1990–2009. *Biogeosciences*, *11*(3), 709–734. https://doi.org/10.5194/bg-11-709-2014

Ishii, M., Rodgers, K. B., Inoue, H. Y., Toyama, K., Sasano, D., Kosugi, N., et al. (2020). Ocean acidification from below in the tropical Pacific. *Global Biogeochemical Cycles*, *34*(8). https://doi.org/10.1029/2019gb006368

Ito, T., Bracco, A., Deutsch, C., Frenzel, H., Long, M., & Takano, Y. (2015). Sustained growth of the Southern Ocean carbon storage in a warming climate. *Geophysical Research Letters*, *42*(11), 4516–4522. https://doi.org/10.1002/2015gl064320

Ito, T., Woloszyn, M., & Mazloff, M. (2010). Anthropogenic carbon dioxide transport in the Southern Ocean driven by Ekman flow. *Nature*, *463*(7277), 80–83. https://doi.org/10.1038/nature08687

Iudicone, D., Rodgers, K. B., Plancherel, Y., Aumont, A., Ito, T., Key, R. M., et al. (2016). The formation of the ocean's anthropogenic carbon reservoir. *Scientific Reports*, *6*(1), 35473. https://doi.org/10.1038/srep35473

Jacobson, A. R., Mikaloff Fletcher, S. E., Gruber, N., Sarmiento, J. L., & Gloor, M. (2007). A joint atmosphere-ocean inversion for surface fluxes of carbon dioxide: 1. Methods and global-scale fluxes. *Global Biogeochemical Cycles*, *21*(1). https://doi.org/10.1029/2005gb002556

Jones, J. M., Gille, S. T., Goosse, H., Abram, N. J., Canziani, P. O., Charman, D. J., et al. (2016). Assessing recent trends in high-latitude Southern Hemisphere surface climate. *Nature Climate Change*, *6*(10), 917–926. https://doi.org/10.1038/nclimate3103

Joos, F., Plattner, G.-K., Stocker, T. F., Marchal, O., & Schmittner, A. (1999). Global warming and marine carbon cycle feedbacks on future atmospheric CO_2. *Science*, *284*(5413), 464–467. https://doi.org/10.1126/science.284.5413.464

Keeling, C. D. (1979). The Suess effect: ^{13}Carbon-^{14}Carbon interrelations. *Environment International*, *2*(4–6), 229–300. https://doi.org/10.1016/0160-4120(79)90005-9

Keeling, C. D., & Revelle, R. (1985). Effects of El Niño/Southern Oscillation on the atmospheric content of carbon dioxide. *Meteoritics*, *20*, 437–450.

Keeling, R. F., Piper, S. C., & Heimann, M. (1996). Global and hemispheric CO_2 sinks deduced from changes in atmospheric O_2 concentration. *Nature*, *381*(6579), 218–221. https://doi.org/10.1038/381218a0

Khatiwala, S., Primeau, F., & Hall, T. (2009). Reconstruction of the history of anthropogenic CO_2 concentrations in the ocean. *Nature*, *462*(7271), 346–349. https://doi.org/10.1038/nature08526

Khatiwala, S., Tanhua, T., Mikaloff Fletcher, S., Gerber, M., Doney, S. C., Graven, H. D., et al. (2013). Global ocean storage of anthropogenic carbon. *Biogeosciences*, *10*(4), 2169–2191. https://doi.org/10.5194/bg-10-2169-2013

Kwon, E. Y., DeVries, T., Galbraith, E. D., Hwang, J., Kim, G., & Timmermann, A. (2021). Stable carbon isotopes suggest large terrestrial carbon inputs to the global ocean. *Global Biogeochemical Cycles*, *35*(4), e2020GB006684. https://doi.org/10.1029/2020gb006684

Lacroix, F., Ilyina, T., & Hartmann, J. (2020). Oceanic CO_2 outgassing and biological production hotspots induced by pre-industrial river loads of nutrients and carbon in a global modeling approach. *Biogeosciences*, *17*(1), 55–88. https://doi.org/10.5194/bg-17-55-2020

Landschützer, P., Gruber, N., Bakker, D. C., & Schuster, U. (2014). Recent variability of the global ocean carbon sink. *Global Biogeochemical Cycles*, *28*(9), 927–949. https://doi.org/10.1002/2014gb004853

Landschützer, P., Gruber, N., Haumann, F. A., Rödenbeck, C., Bakker, D. C., Van Heuven, S., et al. (2015). The reinvigoration of the Southern Ocean carbon sink. *Science*, *349*(6253), 1221–1224. https://doi.org/10.1126/science.aab2620

Landschützer, P., Laruelle, G. G., Roobaert, A., & Regnier, P. (2020). A uniform pCO_2 climatology combining open and coastal oceans. *Earth System Science Data*, *12*(4), 2537–2553. https://doi.org/10.5194/essd-12-2537-2020

Large, W. G., McWilliams, J. C., & Doney, S. C. (1994). Oceanic vertical mixing: A review and a model with a nonlocal boundary layer parameterization. *Reviews of Geophysics*, *32*(4), 363–403. https://doi.org/10.1029/94rg01872

Lee, K., Choi, S. D., Park, G. H., Wanninkhof, R., Peng, T. H., Key, R. M., et al. (2003). An updated anthropogenic CO_2 inventory in the Atlantic Ocean. *Global Biogeochemical Cycles*, *17*(4). https://doi.org/10.1029/2003gb002067

Le Quéré, C., Orr, J. C., Monfray, P., Aumont, O., & Madec, G. (2007a). Interannual variability of the oceanic sink of CO_2 from 1979 through 1997. *Global Biogeochemical Cycles*, *14*(4), 1247–1265. https://doi.org/10.1029/1999gb900049

Le Quéré, C., Rodenbeck, C., Buitenhuis, E. T., Conway, T. J., Langenfelds, R., Gomez, A., et al. (2007b). Saturation of the Southern Ocean CO_2 sink due to recent climate change. *Science*, *316*(5832), 1735–1738. https://doi.org/10.1126/science.1136188

Le Quéré, C., Takahashi, T., Buitenhuis, E. T., Rödenbeck, C., & Sutherland, S. C. (2010). Impact of climate change and variability on the global oceanic sink of CO_2. *Global Biogeochemical Cycles*, *24*(4). https://doi.org/10.1029/2009gb003599

Liao, E., Resplandy, L., Liu, J., & Bowman, K. W. (2020). Amplification of the ocean carbon sink during El Niños: Role of poleward Ekman transport and influence on atmospheric CO_2. *Global Biogeochemical Cycles*, *34*(9), e2020GB006574. https://doi.org/10.1029/2020gb006574

Lo Monaco, C., Goyet, C., Metzl, N., Poisson, A., & Touratier, F. (2005). Distribution and inventory of anthropogenic CO_2 in the Southern Ocean: Comparison of three data-based methods. *Journal of Geophysical Research*, *110*(C9), C09S02. https://doi.org/10.1029/2004jc002571

Lovenduski, N. S., Gruber, N., Doney, S. C., & Lima, I. D. (2007). Enhanced CO_2 outgassing in the Southern Ocean from a positive phase of the Southern Annular Mode. *Global Biogeochemical Cycles*, *21*(2), GB2026. https://doi.org/10.1029/2006GB002900

Maier-Reimer, E., & Hasselmann, K. (1987). Transport and storage of CO_2 in the ocean——An inorganic ocean-circulation carbon cycle model. *Climate Dynamics*, *2*(2), 63–90. https://doi.org/10.1007/bf01054491

Manning, A., & Keeling, R. F. (2006). Global oceanic and land biotic carbon sinks from the Scripps atmospheric oxygen flask sampling network. *Tellus B: Chemical and Physical Meteorology*, *58*(2), 95–116. https://doi.org/10.1111/j.1600-0889.2006.00175.x

McGillis, W. R., Edson, J. B., Hare, J. E., & Fairall, C. W. (2001). Direct covariance air-sea CO_2 fluxes. *Journal of Geophysical Research*, *106*(C8), 16729–16745. https://doi.org/10.1029/2000jc000506

McKinley, G. A., Fay, A. R., Eddebbar, Y. A., Gloege, L., & Lovenduski, N. S. (2020). External forcing explains recent decadal variability of the ocean carbon sink. *AGU Advances*, *1*(2), e2019AV000149. https://doi.org/10.1029/2019av000149

McKinley, G. A., Fay, A. R., Lovenduski, N. S., & Pilcher, D. J. (2017). Natural variability and anthropogenic trends in the ocean carbon sink. *Annual Review of Marine Science*, *9*(1), 125–150. https://doi.org/10.1146/annurev-marine-010816-060529

McKinley, G. A., Rödenbeck, C., Gloor, M., Houweling, S., & Heimann, M. (2004). Pacific dominance to global air-sea CO_2 flux variability: A novel atmospheric inversion agrees with ocean models. *Geophysical Research Letters*, *31*(22), L22308. https://doi.org/10.1029/2004gl021069

McNeil, B. I., & Matear, R. J. (2013). The non-steady state oceanic CO_2 signal: Its importance, magnitude and a novel way to detect it. *Biogeosciences*, *10*(4), 2219–2228. https://doi.org/10.5194/bg-10-2219-2013

McNeil, B. I., Matear, R. J., Key, R. M., Bullister, J. L., & Sarmiento, J. L. (2003). Anthropogenic CO_2 uptake by the ocean based on the global chlorofluorocarbon data set. *Science*, *299*(5604), 235–239. https://doi.org/10.1126/science.1077429

Mikaloff Fletcher, S. E., Gruber, N., Jacobson, A. R., Doney, S. C., Dutkiewicz, S., Gerber, M., et al. (2006). Inverse estimates of anthropogenic CO_2 uptake, transport, and storage by the ocean. *Global Biogeochemical Cycles*, *20*(2). https://doi.org/10.1029/2005gb002530

Müller, J. D. (2023). RECCAP2-ocean data collection [Dataset]. Zenodo. https://doi.org/10.5281/zenodo.7990823

Müller, J. D., Gruber, N., Carter, B., Feely, R., Ishii, M., Lange, N., et al. (2023). Decadal trends in the oceanic storage of anthropogenic carbon from 1994 to 2014. *AGU Advances*, *4*(4), e2023AV000875. https://doi.org/10.1029/2023av000875

Nickford, S., Palter, J. B., Donohue, K., Fassbender, A. J., Gray, A. R., Long, J., et al. (2022). Autonomous wintertime observations of air-sea exchange in the gulf stream reveal a perfect storm for ocean CO_2 uptake. *Geophysical Research Letters*, *49*(5), e2021GL096805. https://doi.org/10.1029/2021gl096805

Oeschger, H., Siegenthaler, U., Schotterer, U., & Gugelmann, A. (1975). A box diffusion model to study the carbon dioxide exchange in nature. *Tellus*, *27*(2), 168–192. https://doi.org/10.3402/tellusa.v27i2.9900

Olsen, A., Key, R. M., van Heuven, S., Lauvset, S. K., Velo, A., Lin, X., et al. (2016). The Global Ocean Data Analysis Project version 2 (GLODAPv2)—An internally consistent data product for the world ocean. *Earth System Science Data*, *8*, 297–323. https://doi.org/10.5194/essd-8-297-2016

Orr, J. C., Maier-Reimer, E., Mikolajewicz, U., Monfray, P., Sarmiento, J. L., Toggweiler, J. R., et al. (2001). Estimates of anthropogenic carbon uptake from four three-dimensional global ocean models. *Global Biogeochemical Cycles*, *15*(1), 43–60. https://doi.org/10.1029/2000gb001273

Park, G. H., Wanninkhof, R. I. K., Doney, S., Takahashi, T., Lee, K., Feely, R., et al. (2010). Variability of global net sea–air CO_2 fluxes over the last three decades using empirical relationships. *Tellus B: Chemical and Physical Meteorology*, *62*(5), 352–368. https://doi.org/10.3402/tellusb.v62i5.16580

Quay, P. D., Tilbrook, B., & Wong, C. S. (1992). Oceanic uptake of fossil fuel CO_2: Carbon-13 evidence. *Science*, *256*(5053), 74–79. https://doi.org/10.1126/science.256.5053.74

Regnier, P., Friedlingstein, P., Ciais, P., Mackenzie, F. T., Gruber, N., Janssens, I. A., et al. (2013). Anthropogenic perturbation of the carbon fluxes from land to ocean. *Nature Geoscience*, *6*(8), 597–607. https://doi.org/10.1038/ngeo1830

Regnier, P., Resplandy, L., Najjar, R. G., & Ciais, P. (2022). The land-to-ocean loops of the global carbon cycle. *Nature*, *603*(7901), 401–410. https://doi.org/10.1038/s41586-021-04339-9

Resplandy, L., Hogikyan, A., Bange, H. W., Bianchi, D., Weber, T. S., Cai, W. J., et al. (2023). *A synthesis of global coastal ocean greenhouse gas fluxes*. Authorea Preprints.

Resplandy, L., Keeling, R. F., Eddebbar, Y., Brooks, M., Wang, R., Bopp, L., et al. (2019). Quantification of ocean heat uptake from changes in atmospheric O_2 and CO_2 composition. *Scientific Reports*, *9*(1), 20244. https://doi.org/10.1038/s41598-019-56490-z

Resplandy, L., Keeling, R. F., Rödenbeck, C., Stephens, B. B., Khatiwala, S., Rodgers, K. B., et al. (2018). Revision of global carbon fluxes based on a reassessment of oceanic and riverine carbon transport. *Nature Geoscience*, *11*(7), 504–509. https://doi.org/10.1038/s41561-018-0151-3

Revelle, R., & Suess, H. E. (1957). Carbon dioxide exchange between atmosphere and ocean and the question of an increase of atmospheric CO_2 during the past decades. *Tellus*, *9*, 1–10. https://doi.org/10.3402/tellusa.v9i1.9075

Ridge, S. M., & McKinley, G. A. (2020). Advective controls on the North Atlantic anthropogenic carbon sink. *Global Biogeochemical Cycles*, *34*(7), e2019GB006457. https://doi.org/10.1029/2019GB006457

Ridge, S. M., & McKinley, G. A. (2021). Ocean carbon uptake under aggressive emission mitigation. *Biogeosciences*, *18*(8), 2711–2725. https://doi.org/10.5194/bg-18-2711-2021

Rödenbeck, C., Bakker, D. C., Gruber, N., Iida, Y., Jacobson, A. R., Jones, S., et al. (2015). Data-based estimates of the ocean carbon sink variability–first results of the surface ocean pCO_2 mapping intercomparison (SOCOM). *Biogeosciences*, *12*(23), 7251–7278. https://doi.org/10.5194/bg-12-7251-2015

Rödenbeck, C., DeVries, T., Hauck, J., Le Quéré, C., & Keeling, R. F. (2022). Data-based estimates of interannual sea–air CO_2 flux variations 1957–2020 and their relation to environmental drivers. *Biogeosciences*, *19*(10), 2627–2652. https://doi.org/10.5194/bg-19-2627-2022

Rödenbeck, C., Keeling, R. F., Bakker, D. C., Metzl, N., Olsen, A., Sabine, C., & Heimann, M. (2013). Global surface-ocean pCO_2 and sea–air CO_2 flux variability from an observation-driven ocean mixed-layer scheme. *Ocean Science*, *9*(2), 193–216. https://doi.org/10.5194/os-9-193-2013

Rodgers, K. B., Sarmiento, J. L., Aumont, O., Crevoisier, C., de Boyer Montégut, C., & Metzl, N. (2008). A wintertime uptake window for anthropogenic CO_2 in the North Pacific. *Global Biogeochemical Cycles*, *22*(2). https://doi.org/10.1029/2006gb002920

Rodgers, K. B., Schwinger, J., Fassbender, A. J., Landschützer, P., Yamaguchi, R., Frenzel, H., et al. (2023). Seasonal variability of the surface ocean carbon cycle: A synthesis. *Global Biogeochemical Cycles*, *37*, e2023GB007798. https://doi.org/10.1029/2023GB007798

Roobaert, A., Laruelle, G. G., Landschützer, P., Gruber, N., Chou, L., & Regnier, P. (2019). The spatiotemporal dynamics of the sources and sinks of CO_2 in the global coastal ocean. *Global Biogeochemical Cycles*, *33*(12), 1693–1714. https://doi.org/10.1029/2019gb006239

Roobaert, A., Laruelle, G. G., Landschützer, P., & Regnier, P. (2018). Uncertainty in the global oceanic CO_2 uptake induced by wind forcing: Quantification and spatial analysis. *Biogeosciences*, *15*(6), 1701–1720. https://doi.org/10.5194/bg-15-1701-2018

Roobaert, A., Regnier, P., Landschützer, P., & Laruelle, G. G. (2023). A novel sea surface pCO_2-product for the global coastal ocean resolving trends over the 1982–2020 period. *Earth System Science Data Discussions*, *2023*, 1–32.

Roobaert, A., Resplandy, L., Laruelle, G. G., Liao, E., & Regnier, P. (2022). A framework to evaluate and elucidate the driving mechanisms of coastal sea surface pCO_2 seasonality using an ocean general circulation model (MOM6-COBALT). *Ocean Science*, *18*(1), 67–88. https://doi.org/10.5194/os-18-67-2022

Sabine, C. L., Feely, R. A., Gruber, N., Key, R. M., Lee, K., Bullister, J. L., et al. (2004). The oceanic sink for anthropogenic CO_2. *Science*, *305*(5682), 367–371. https://doi.org/10.1126/science.1097403

Sarmiento, J. L., Orr, J. C., & Siegenthaler, U. (1992). A perturbation simulation of CO_2 uptake in an ocean general circulation model. *Journal of Geophysical Research*, *97*(C3), 3621–3645. https://doi.org/10.1029/91jc02849

Schwinger, J., Tjiputra, J. F., Heinze, C., Bopp, L., Christian, J. R., Gehlen, M., et al. (2014). Nonlinearity of ocean carbon cycle feedbacks in CMIP5 earth system models. *Journal of Climate*, *27*(11), 3869–3888. https://doi.org/10.1175/jcli-d-13-00452.1

Séférian, R., Gehlen, M., Bopp, L., Resplandy, L., Orr, J. C., Marti, O., et al. (2016). Inconsistent strategies to spin up models in CMIP5: Implications for ocean biogeochemical model performance assessment. *Geoscientific Model Development*, *9*(5), 1827–1851. https://doi.org/10.5194/gmd-9-1827-2016

Séférian, R., Ribes, A., & Bopp, L. (2014). Detecting the anthropogenic influences on recent changes in ocean carbon uptake. *Geophysical Research Letters*, *41*(16), 5968–5977. https://doi.org/10.1002/2014gl061223

Sharp, J. D., Fassbender, A. J., Carter, B. R., Lavin, P. D., & Sutton, A. J. (2022). A monthly surface pCO_2 product for the California Current Large Marine Ecosystem. *Earth System Science Data*, *14*(4), 2081–2108. https://doi.org/10.5194/essd-14-2081-2022

Shin, Y., Deike, L., & Romero, L. (2022). Modulation of bubble-mediated CO_2 gas transfer due to wave-current interactions. *Geophysical Research Letters*, *49*(22), e2022GL100017. https://doi.org/10.1029/2022gl100017

Siegenthaler, U., & Sarmiento, J. L. (1993). Atmospheric carbon dioxide and the ocean. *Nature*, *365*(6442), 119–125. https://doi.org/10.1038/365119a0

Steinfeldt, R., Rhein, M., Bullister, J. L., & Tanhua, T. (2009). Inventory changes in anthropogenic carbon from 1997–2003 in the Atlantic Ocean between 20 S and 65 N. *Global Biogeochemical Cycles*, *23*(3). https://doi.org/10.1029/2008gb003311

Sutton, A. J., Feely, R. A., Maenner-Jones, S., Musielwicz, S., Osborne, J., Dietrich, C., et al. (2019). Autonomous seawater pCO_2 and pH time series from 40 surface buoys and the emergence of anthropogenic trends. *Earth System Science Data*, *11*(1), 421–439. https://doi.org/10.5194/essd-11-421-2019

Sutton, A. J., Williams, N. L., & Tilbrook, B. (2021). Constraining Southern Ocean CO_2 flux uncertainty using uncrewed surface vehicle observations. *Geophysical Research Letters*, *48*(3), e2020GL091748. https://doi.org/10.1029/2020gl091748

Swart, N. C., & Fyfe, J. C. (2012). Observed and simulated changes in the Southern Hemisphere surface westerly wind-stress. *Geophysical Research Letters*, *39*(16), L16711. https://doi.org/10.1029/2012gl052810

Takahashi, T., Feely, R. A., Weiss, R. F., Wanninkhof, R. H., Chipman, D. W., Sutherland, S. C., & Takahashi, T. T. (1997). Global air-sea flux of CO_2: An estimate based on measurements of sea–air pCO_2 difference. *Proceedings of the National Academy of Sciences of the United States of America*, *94*(16), 8292–8299. https://doi.org/10.1073/pnas.94.16.8292

Takahashi, T., Sutherland, S. C., Sweeney, C., Poisson, A., Metzl, N., Tilbrook, B., et al. (2002). Global sea–air CO_2 flux based on climatological surface ocean pCO_2, and seasonal biological and temperature effects. *Deep Sea Research Part II: Topical Studies in Oceanography*, *49*(9–10), 1601–1622. https://doi.org/10.1016/s0967-0645(02)00003-6

Takahashi, T., Sutherland, S. C., Wanninkhof, R., Sweeney, C., Feely, R. A., Chipman, D. W., et al. (2009). Climatological mean and decadal change in surface ocean pCO_2, and net sea–air CO_2 flux over the global oceans. *Deep Sea Research Part II: Topical Studies in Oceanography*, *56*(8–10), 554–577. https://doi.org/10.1016/j.dsr2.2008.12.009

Talley, L. D., Feely, R. A., Sloyan, B. M., Wanninkhof, R., Baringer, M. O., Bullister, J. L., et al. (2016). Changes in ocean heat, carbon content, and ventilation: A review of the first decade of GO-SHIP global repeat hydrography. *Annual Review of Marine Science*, *8*(1), 185–215. https://doi.org/10.1146/annurev-marine-052915-100829

Taylor, K. E., Stouffer, R. J., & Meehl, G. A. (2012). An overview of CMIP5 and the experiment design. *Bulletin of the American Meteorological Society*, *93*(4), 485–498. https://doi.org/10.1175/bams-d-11-00094.1

Terhaar, J., Frölicher, T. L., & Joos, F. (2021). Southern Ocean anthropogenic carbon sink constrained by sea surface salinity. *Science Advances*, *7*(18), eabd5964. https://doi.org/10.1126/sciadv.abd5964

Terhaar, J., Frölicher, T. L., & Joos, F. (2022). Observation-constrained estimates of the global ocean carbon sink from Earth system models. *Biogeosciences*, *19*(18), 4431–4457. https://doi.org/10.5194/bg-19-4431-2022

Terhaar, J., Goris, N., Müller, J. D., DeVries, T., Gruber, N., Hauck, J., et al. (2023). Assessment of global ocean biogeochemistry models for ocean carbon sink estimates in RECCAP2 and recommendations for future studies.

Toyama, K., Rodgers, K. B., Blanke, B., Iudicone, D., Ishii, M., Aumont, O., & Sarmiento, J. L. (2017). Large reemergence of anthropogenic carbon into the ocean's surface mixed layer sustained by the ocean's overturning circulation. *Journal of Climate*, *30*(21), 8615–8631. https://doi.org/10.1175/jcli-d-16-0725.1

Vázquez-Rodríguez, M., Touratier, F., lo Monaco, C., Waugh, D. W., Padin, X. A., Bellerby, R. G. J., et al. (2009). Anthropogenic carbon distributions in the Atlantic Ocean: Data-based estimates from the Arctic to the Antarctic. *Biogeosciences*, *6*(3), 439–451. https://doi.org/10.5194/bg-6-439-2009

Wanninkhof, R. (2007). The impact of different gas exchange formulations and wind speed products on global air-sea CO_2 fluxes. In C. S. Garbe, R. A. Handler, & B. Jaehne (Eds.), *Transport at the air sea interface, measurements, models and parametrizations* (pp. 1–23). Springer.

Wanninkhof, R., Asher, W. E., Ho, D. T., Sweeney, C. S., & McGillis, W. R. (2009). Advances in quantifying air-sea gas exchange and environmental forcing. *Annual Review of Marine Science*, *1*, 213–244. https://doi.org/10.1146/annurev.marine.010908.163742

Wanninkhof, R., & McGillis, W. R. (1999). A cubic relationship between air-sea CO_2 exchange and wind speed. *Geophysical Research Letters*, *26*(13), 1889–1892. https://doi.org/10.1029/1999gl900363

Wanninkhof, R., Park, G. H., Takahashi, T., Sweeney, C., Feely, R., Nojiri, Y., et al. (2013). Global ocean carbon uptake: Magnitude, variability and trends. *Biogeosciences*, *10*(3), 1983–2000. https://doi.org/10.5194/bg-10-1983-2013

Wanninkhof, R., Pickers, P. A., Omar, A. M., Sutton, A., Murata, A., Olsen, A., et al. (2019). A surface ocean CO_2 reference network, SOCONET and associated marine boundary layer CO_2 measurements. *Frontiers in Marine Science*, *6*, 400. https://doi.org/10.3389/fmars.2019.00400

Wanninkhof, R., & Triñanes, J. (2017). The impact of changing wind speeds on gas transfer and its effect on global air-sea CO_2 fluxes. *Global Biogeochemical Cycles*, *31*(6), 961–974. https://doi.org/10.1002/2016gb005592

Watson, A. J., Schuster, U., Shutler, J. D., Holding, T., Ashton, I. G., Landschützer, P., et al. (2020). Revised estimates of ocean-atmosphere CO_2 flux are consistent with ocean carbon inventory. *Nature Communications*, *11*(1), 1–6. https://doi.org/10.1038/s41467-020-18203-3

Watts, J., Bell, T. G., Anderson, K., Butterworth, B. J., Miller, S., Else, B., & Shutler, J. (2022). Impact of sea ice on air-sea CO_2 exchange–A critical review of polar eddy covariance studies. *Progress in Oceanography*, *201*, 102741. https://doi.org/10.1016/j.pocean.2022.102741

Waugh, D. W., Hall, T. M., McNeil, B. I., Key, R., & Matear, R. J. (2006). Anthropogenic CO_2 in the oceans estimated using transit time distributions. *Tellus B: Chemical and Physical Meteorology*, *58*(5), 376–389. https://doi.org/10.3402/tellusb.v58i5.17030

Waugh, D. W., Primeau, F., DeVries, T., & Holzer, M. (2013). Recent changes in the ventilation of the southern oceans. *Science*, *339*(6119), 568–570. https://doi.org/10.1126/science.1225411

Woolf, D. K., Shutler, J. D., Goddijn-Murphy, L., Watson, A. J., Chapron, B., Nightingale, P. D., et al. (2019). Key uncertainties in the recent air-sea flux of CO_2. *Global Biogeochemical Cycles*, *33*(12), 1548–1563. https://doi.org/10.1029/2018gb006041

Zelinka, M. D., Myers, T. A., McCoy, D. T., Po-Chedley, S., Caldwell, P. M., Ceppi, P., et al. (2020). Causes of higher climate sensitivity in CMIP6 models. *Geophysical Research Letters*, *47*(1), e2019GL085782. https://doi.org/10.1029/2019gl085782

Zeng, J., Iida, Y., Matsunaga, T., & Shirai, T. (2022). Surface ocean CO_2 concentration and air-sea flux estimate by machine learning with modelled variable trends. *Frontiers in Marine Science*, *9*, 0–14. https://doi.org/10.3389/fmars.2022.989233

Zhang, H., Menemenlis, D., & Fenty, I. (2018). ECCO LLC270 ocean-ice state estimate.

References From the Supporting Information

Aumont, O., Ethé, C., Tagliabue, A., Bopp, L., & Gehlen, M. (2015). PISCES-v2: An ocean biogeochemical model for carbon and ecosystem studies. *Geoscientific Model Development*, *8*, 2465–2513. https://doi.org/10.5194/gmd-8-2465-2015

Ballantyne, A. Á., Alden, C. Á., Miller, J. Á., Tans, P. Á., & White, J. W. C. (2012). Increase in observed net carbon dioxide uptake by land and oceans during the past 50 years. *Nature*, *488*(7409), 70–72. https://doi.org/10.1038/nature11299

Berthet, S., Séférian, R., Bricaud, C., Chevallier, M., Voldoire, A., & Ethé, C. (2019). Evaluation of an online grid-coarsening algorithm in a global eddy-admitting ocean-biogeochemical model. *Journal of Advances in Modeling Earth Systems*, *11*(6), 1759–1783. https://doi.org/10.1029/2019ms001644

Chien, C. T., Durgadoo, J., Ehlers, D., Keller, D., Koeve, W., Kriest, I., et al. (2022). FOCI-MOPS v1—Integration of marine biogeochemistry within the Flexible Ocean and Climate Infrastructure version 1 (FOCI 1) Earth system model. *Geoscientific Model Development*, *15*, 5987–6024. https://doi.org/10.5194/gmd-15-5987-2022

Cooper, D. J., Watson, A. J., & Ling, R. D. (1998). Variation of pCO_2 along a North Atlantic shipping route (UK to the Caribbean): A year of automated observations. *Marine Chemistry*, *60*(1–2), 147–164. https://doi.org/10.1016/s0304-4203(97)00082-0

Dickson, A. G., Sabine, C. L., & Christian, J. R. (2007). *Guide to best practices for ocean CO_2 measurements*. North Pacific Marine Science Organization.

Doney, S. C., Lima, I., Feely, R. A., Glover, D. M., Lindsay, K., Mahowald, N., et al. (2009). Mechanisms governing interannual variability in upper-ocean inorganic carbon system and air–sea CO_2 fluxes: Physical climate and atmospheric dust. *Deep Sea Research Part II: Topical Studies in Oceanography*, *56*(8–10), 640–655. https://doi.org/10.1016/j.dsr2.2008.12.006

Döscher, R., Acosta, M., Alessandri, A., Anthoni, P., Arsouze, T., Bergman, T., et al. (2022). The EC-Earth3 Earth system model for the coupled model intercomparison project 6. *Geoscientific Model Development*, *15*(7), 2973–3020. https://doi.org/10.5194/gmd-15-2973-2022

Goddijn-Murphy, L. M., Woolf, D. K., Land, P. E., Shutler, J. D., & Donlon, C. (2015). The OceanFlux Greenhouse Gases methodology for deriving a sea surface climatology of CO_2 fugacity in support of air–sea gas flux studies. *Ocean Science*, *11*(4), 519–541. https://doi.org/10.5194/os-11-519-2015

Gregor, L., & Gruber, N. (2021). OceanSODA-ETHZ: A global gridded data set of the surface ocean carbonate system for seasonal to decadal studies of ocean acidification. *Earth System Science Data*, *13*(2), 777–808. https://doi.org/10.5194/essd-13-777-2021

Hauck, J., Gregor, L., Nissen, C., Patara, L., Hague, M., Mongwe, P., et al. (2023b). The Southern Ocean carbon cycle 1985-2018: Mean, seasonal cycle, trends and storage. *Authorea Preprints*.

Ilyina, T., Six, K. D., Segschneider, J., Maier-Reimer, E., Li, H., & Núñez-Riboni, I. (2013). Global ocean biogeochemistry model HAMOCC: Model architecture and performance as component of the MPI-Earth system model in different CMIP5 experimental realizations. *Journal of Advances in Modeling Earth Systems*, *5*(2), 287–315. https://doi.org/10.1029/2012ms000178

Joos, F., & Spahni, R. (2008). Rates of change in natural and anthropogenic radiative forcing over the past 20,000 years. *Proceedings of the National Academy of Sciences of the United States of America*, *105*(5), 1425–1430. https://doi.org/10.1073/pnas.0707386105

Kriest, I., & Oschlies, A. (2015). MOPS-1.0: Towards a model for the regulation of the global oceanic nitrogen budget by marine biogeochemical processes. *Geoscientific Model Development*, *8*(9), 2929–2957. https://doi.org/10.5194/gmd-8-2929-2015

Landschützer, P., Gruber, N., & Bakker, D. C. (2016). Decadal variations and trends of the global ocean carbon sink. *Global Biogeochemical Cycles*, *30*(10), 1396–1417. https://doi.org/10.1002/2015gb005359

Le Quéré, C., Buitenhuis, E. T., Moriarty, R., Alvain, S., Aumont, O., Bopp, L., et al. (2016). Role of zooplankton dynamics for Southern Ocean phytoplankton biomass and global biogeochemical cycles. *Biogeosciences*, *13*(14), 4111–4133. https://doi.org/10.5194/bg-13-4111-2016

Lindsay, K., Bonan, G. B., Doney, S. C., Hoffman, F. M., Lawrence, D. M., Long, M. C., et al. (2014). Preindustrial-control and twentieth-century carbon cycle experiments with the Earth System Model CESM1(BGC). *Journal of Climate*, *27*(24), 8981–9005. https://doi.org/10.1175/jcli-d-12-00565.1

Mauritsen, T., Bader, J., Becker, T., Behrens, J., Bittner, M., Brokopf, R., et al. (2019). Developments in the MPI-M Earth system model version 1.2 (MPI-ESM1. 2) and its response to increasing CO_2. *Journal of Advances in Modeling Earth Systems*, *11*(4), 998–1038. https://doi.org/10.1029/2018ms001400

Meinshausen, M., Vogel, E., Nauels, A., Lorbacher, K., Meinshausen, N., Etheridge, D. M., et al. (2017). Historical greenhouse gas concentrations for climate modelling (CMIP6). *Geoscientific Model Development*, *10*(5), 2057–2116. https://doi.org/10.5194/gmd-10-2057-2017

Nightingale, P. D., Malin, G., Law, C. S., Watson, A. J., Liss, P. S., Liddicoat, M. I., et al. (2000). In situ evaluation of air-sea gas exchange parameterizations using novel conservative and volatile tracers. *Global Biogeochemical Cycles*, *14*(1), 373–387. https://doi.org/10.1029/1999gb900091

Pierrot, D., Neill, C., Sullivan, K., Castle, R., Wanninkhof, R., Lüger, H., et al. (2009). Recommendations for autonomous underway pCO_2 measuring systems and data-reduction routines. *Deep Sea Research Part II: Topical Studies in Oceanography*, *56*(8–10), 512–522. https://doi.org/10.1016/j.dsr2.2008.12.005

Sarma, V., Sridevi, B., Metzl, N., Patra, P. K., Lachkar, Z., Chakraborty, K., et al. (2023). Air-sea fluxes of CO_2 in the Indian Ocean between 1985 and 2018: A synthesis based on observation-based surface CO_2, hindcast and atmospheric inversion models. *Global Biogeochemical Cycles*, *37*(5), e2023GB007694. https://doi.org/10.1029/2023gb007694

Schwinger, J., Goris, N., Tjiputra, J. F., Kriest, I., Bentsen, M., Bethke, I., et al. (2016). Evaluation of NorESM-OC (versions 1 and 1.2), the ocean carbon-cycle stand-alone configuration of the Norwegian Earth System Model (NorESM1). *Geoscientific Model Development*, *9*(8), 2589–2622. https://doi.org/10.5194/gmd-9-2589-2016

Séférian, R., Berthet, S., Yool, A., Palmiéri, J., Bopp, L., Tagliabue, A., et al. (2020). Tracking improvement in simulated marine biogeochemistry between CMIP5 and CMIP6. *Current Climate Change Reports*, *6*(3), 95–119. https://doi.org/10.1007/s40641-020-00160-0

Séférian, R., Nabat, P., Michou, M., Saint-Martin, D., Voldoire, A., Colin, J., et al. (2019). Evaluation of CNRM Earth-System model, CNRM-ESM2-1: Role of Earth system processes in present-day and future climate. *Journal of Advances in Modeling Earth Systems*, *11*(12), 4182–4227. https://doi.org/10.1029/2019ms001791

Sein, D. V., Koldunov, N. V., Danilov, S., Sidorenko, D., Wekerle, C., Cabos, W., et al. (2018). The relative influence of atmospheric and oceanic model resolution on the circulation of the North Atlantic Ocean in a coupled climate model. *Journal of Advances in Modeling Earth Systems*, *10*(8), 2026–2041. https://doi.org/10.1029/2018ms001327

Stock, C. A., Dunne, J. P., Fan, S., Ginoux, P., John, J., Krasting, J. P., et al. (2020). Ocean biogeochemistry in GFDL's Earth system model 4.1 and its response to increasing atmospheric CO_2. *Journal of Advances in Modeling Earth Systems*, *12*(10), e2019MS002043. https://doi.org/10.1029/2019ms002043

Tsujino, H., Nakano, H., Sakamoto, K., Urakawa, S., Hirabara, M., Ishizaki, H., & Yamanaka, G. (2017). *Reference manual for the meteorological research institute community ocean model version 4 (MRI. COMv4)* (Vol. 80, p. 306). Technical Reports of the Meteorological Research Institute.

Urakawa, L. S., Tsujino, H., Nakano, H., Sakamoto, K., Yamanaka, G., & Toyoda, T. (2020). The sensitivity of a depth-coordinate model to diapycnal mixing induced by practical implementations of the isopycnal tracer diffusion scheme. *Ocean Modelling*, *154*, 101693. https://doi.org/10.1016/j.ocemod.2020.101693

Wanninkhof, R. (1992). Relationship between wind speed and gas exchange over the ocean. *Journal of Geophysical Research*, *97*(C5), 7373–7382. https://doi.org/10.1029/92jc00188

Wanninkhof, R. (2014). Relationship between wind speed and gas exchange over the ocean revisited. *Limnology and Oceanography: Methods*, *12*(6), 351–362. https://doi.org/10.4319/lom.2014.12.351

Weiss, R. F., & Price, B. A. (1980). Nitrous oxide solubility in water and seawater. *Marine Chemistry*, *8*(4), 347–359. https://doi.org/10.1016/0304-4203(80)90024-9

Wright, R. M., Le Quéré, C., Buitenhuis, E., Pitois, S., & Gibbons, M. J. (2021). Role of jellyfish in the plankton ecosystem revealed using a global ocean biogeochemical model. *Biogeosciences*, *18*(4), 1291–1320. https://doi.org/10.5194/bg-18-1291-2021

Yang, S., & Gruber, N. (2016). The anthropogenic perturbation of the marine nitrogen cycle by atmospheric deposition: Nitrogen cycle feedbacks and the 15N Haber-Bosch effect. *Global Biogeochemical Cycles*, *30*(10), 1418–1440. https://doi.org/10.1002/2016gb005421

Yasunaka, S., Manizza, M., Terhaar, J., Olsen, A., Yamaguchi, R., Landschützer, P., et al. (2023). *An assessment of CO_2 uptake in the Arctic Ocean from 1985 to 2018*. Authorea Preprints.